Plants in Action ADAPTATION IN NATURE, PERFORMANCE IN CULTIVATION Edition 1
Published on *Plants in Action* (http://plantsinaction.science.uq.edu.au/edition1)

Chapter 1 - Light use and leaf gas exchange

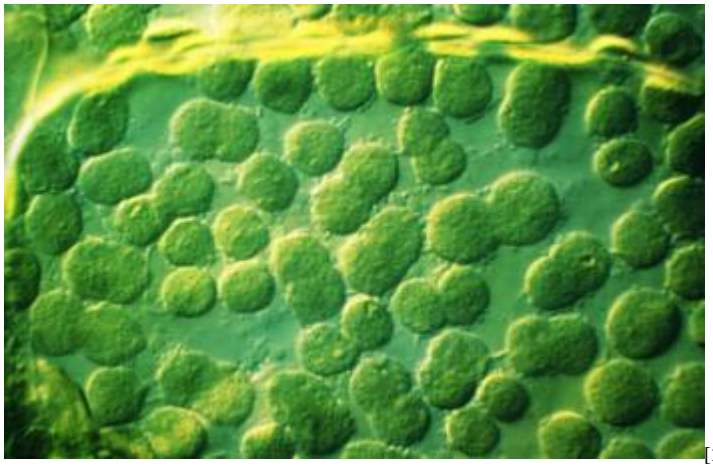 [1]

Chloroplasts dividing (dumbell figures) within an enlarging cell of a young spinach leaf, resulting in about 200 chloroplasts per cell at leaf maturity (Nomarski optics). (Light micrograph courtesy John Possingham)

...leaves seem also designed for many other noble and important services, plants very probably drawing thro' their leaves some part of their nourishment from the air. May not light also, by freely entring the expanded surfaces of leaves and flowers, contribute much to ... ennobling the principles of vegetables?...

(Stephen Hales, Vegetable Staticks, 1727)

Introduction

Leaves epitomise adaptive responses in vascular plants where environment alters expression of genes encoding both form and function. Endless variations in leaf size, shape and pose attest adaptation in form, while qualitative differences in photosynthetic mode reflect contrasting function.

Despite such variation, leaves fulfil a common purpose: to capture energy from sunlight and convert that currency into chemically useful forms to drive CO_2 assimilation and subsequent growth. Light absorption and energy utilisation is considered at progressively finer levels of organisation from leaves (Section 1.1) to chloroplasts (Section 1.2).

Section 1.1 encompasses anatomy, light interception and leaf gas exchange and includes a case study on development of a process-based model for photosynthetic CO_2 assimilation using A:p_i curves.

1.1 - Leaf anatomy, light interception and gas exchange

Leaves have evolved into a myriad of sizes and shapes, showing great variation in surface features and internal anatomy. Nevertheless, these organs all share a common function, namely to intercept sunlight and facilitate CO_2 uptake while restricting water loss. The wide variety of shapes, sizes and internal structure that leaves display implies that many solutions exist to meet the mixed demands of leaf function under frequently adverse conditions.

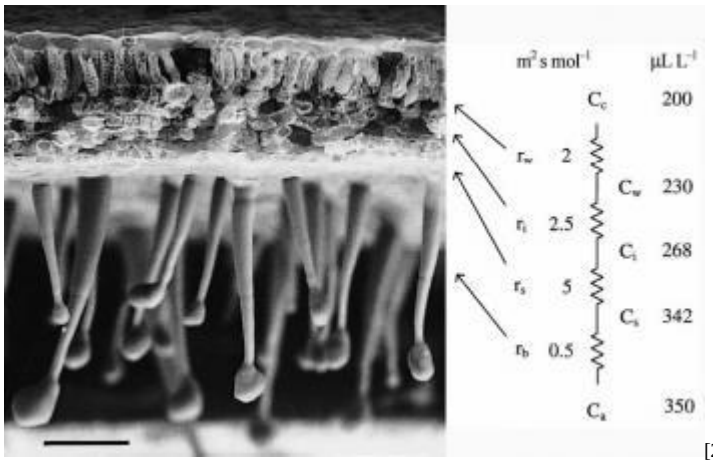

[2]

Figure 1.1 A scanning electron micrograph of an uncoated and rapidly frozen piece of tobacco leaf showing a hairy lower leaf surface and cross-sectional anatomy at low magnification. Epidermal outgrowths (hairs) offer some protection against insects, and contribute to formation of a boundary layer (unstirred air) adjacent to lower leaf surfaces. An electrical analogue (right side) shows a series of resistances (*r*) that would be experienced by CO_2 molecules diffusing from outside (ambient) air to fixation sites inside chloroplasts. Subscript 'b' refers to boundary layer, 's' to stomatal, 'i' to intercellular airspaces, 'w' to cell wall and liquid phase. Notional values for these resistances are given in units of m^2 s mol^{-1}, and emphasise the prominence of stomatal resistance within this series. Corresponding values for CO_2 concentration are shown in µL L^{-1}, and reflect photosynthetic assimilation within leaves generating a gradient for inward diffusion. In that case, subscript 'a' refers to ambient air, 's' to leaf surface, 'i' to substomatal cavity, 'w' to mesophyll cell wall surface, 'c' to sites of carboxylation within chloroplasts. c_i is routinely inferred from gas exchange measurements and used to construct A:$c_i$curves for leaf photosynthesis. Scale bar = 100 µm. (Original illustration from Jian-Wei Yu and John Evans, unpublished)

In nature, photon irradiance (photon flux density) can fluctuate over three orders of magnitude and these changes can be rapid. However, plants have evolved with photosynthetic systems that operate most efficiently at low light. Such efficiency

confers an obvious selective advantage under light limitation, but predisposes to photodamage under strong light. How then can leaves cope? First, some tolerance is achieved by distributing light over a large population of chloroplasts held in architectural arrays within mesophyll tissues. Second, each chloroplast can operate as a seemingly independent entity with respect to photochemistry and biochemistry and can vary allocation of resources between photon capture and capacity for CO_2 assimilation in response to light climate. Such features confer great flexibility across a wide range of light environments where plants occur and are discussed in Chapter 12.

Photon absorption is astonishingly fast (single events lasting 10^{-15} s). Subsequent energy transduction into NADPH and ATP is relatively 'slow' (10^{-4} s), and is followed by CO_2 fixation via Rubisco at a sedate pace of 3.5 events per second per active site, and is generally constrained by even slower diffusion processes. Distributing light absorption between many chloroplasts thus equalises effort over a huge population of these organelles, but also reduces diffusion limitations by allowing placement of chloroplasts at optimal locations within each cell. The internal structure of leaves (Figures 1.1 and 1.2) reflects this need to maximise CO_2 exchange between intercellular airspace and chloroplasts and to distribute light more uniformly with depth than would occur in an homogeneous solution of chlorophyll.

1.1.1 - Leaf Structure

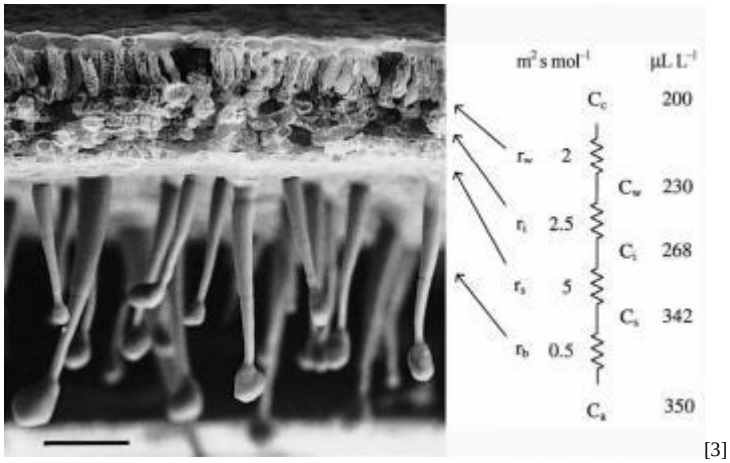

[3]

Figure 1.1 A scanning electron micrograph of an uncoated and rapidly frozen piece of tobacco leaf showing a hairy lower leaf surface and cross-sectional anatomy at low magnification. Epidermal outgrowths (hairs) offer some protection against insects, and contribute to formation of a boundary layer (unstirred air) adjacent to lower leaf surfaces. An electrical analogue (right side) shows a series of resistances (*r*) that would be experienced by CO_2 molecules diffusing from outside (ambient) air to fixation sites inside chloroplasts. Subscript 'b' refers to boundary layer, 's' to stomatal, 'i' to intercellular airspaces, 'w' to cell wall and liquid phase. Notional values for these resistances are given in units of m^2 s mol^{-1}, and emphasise the prominence of stomatal resistance within this series. Corresponding values for CO_2 concentration are shown in µL L^{-1},

and reflect photosynthetic assimilation within leaves generating a gradient for inward diffusion. In that case, subscript 'a' refers to ambient air, 's' to leaf surface, 'i' to substomatal cavity, 'w' to mesophyll cell wall surface, 'c' to sites of carboxylation within chloroplasts. c_i is routinely inferred from gas exchange measurements and used to construct A:$c_i$curves for leaf photosynthesis. Scale bar = 100 µm. (Original illustration from Jian-Wei Yu and John Evans, unpublished)

In a typical herbaceous dicotyledon (Figure 1.1) lower leaf surfaces are covered with epidermal outgrowths, known to impede movement of small insects, but also contributing to formation of a boundary layer. This unstirred zone immediately adjacent to upper and lower epidermes varies in thickness according to surface relief, area and wind speed. Boundary layers are significant in leaf heat budgets and feature in the calculation of stomatal and internal conductances from measurements of leaf gas exchange.

In transverse fracture (Figure 1.2A) the bifacial nature of leaf mesophyll is apparent with columnar palisade cells beneath the upper surface and irregular shaped cells forming the spongy mesophyll below. Large intercellular airspaces, particularly in the spongy mesophyll, facilitate gaseous diffusion. The lower surface of this leaf is shown in Figure 1.2B. On the left-hand side, the epidermis is present with its irregular array of stomata. Diagonally through the centre is a vein with broken-off hair cells and on the right the epidermis has been fractured off revealing spongy mesophyll cells. Light micrographs of sections cut parallel to the leaf surface (paradermal) through palisade (C) and spongy (D) tissue reveal chloroplasts lying in a single layer and covering most of the internal cell wall surface adjacent to airspaces. Significantly, they are rarely present on walls that adjoin another cell. Despite the appearance of close packing, palisade cell surfaces are generally exposed to intercellular airspace. Inward diffusion of CO_2 to chloroplasts is thereby facilitated.

Leaves that develop in sunny environments and have high photosynthetic capacities are generally thicker than leaves from shaded environments. This is achieved with more elongate palisade cells and/or several layers of palisade cells. Thicker leaves in a sunny environment prove energy effective because enough photons reach chloroplasts in lower cell layers to keep their Rubisco gainfully employed. Such depth deploys sufficient Rubisco to confer a high photosynthetic capacity. By contrast, in a shaded habitiat, less Rubisco is required for a leaf with lower photosynthetic capacity, and this can be achieved with thinner leaves.

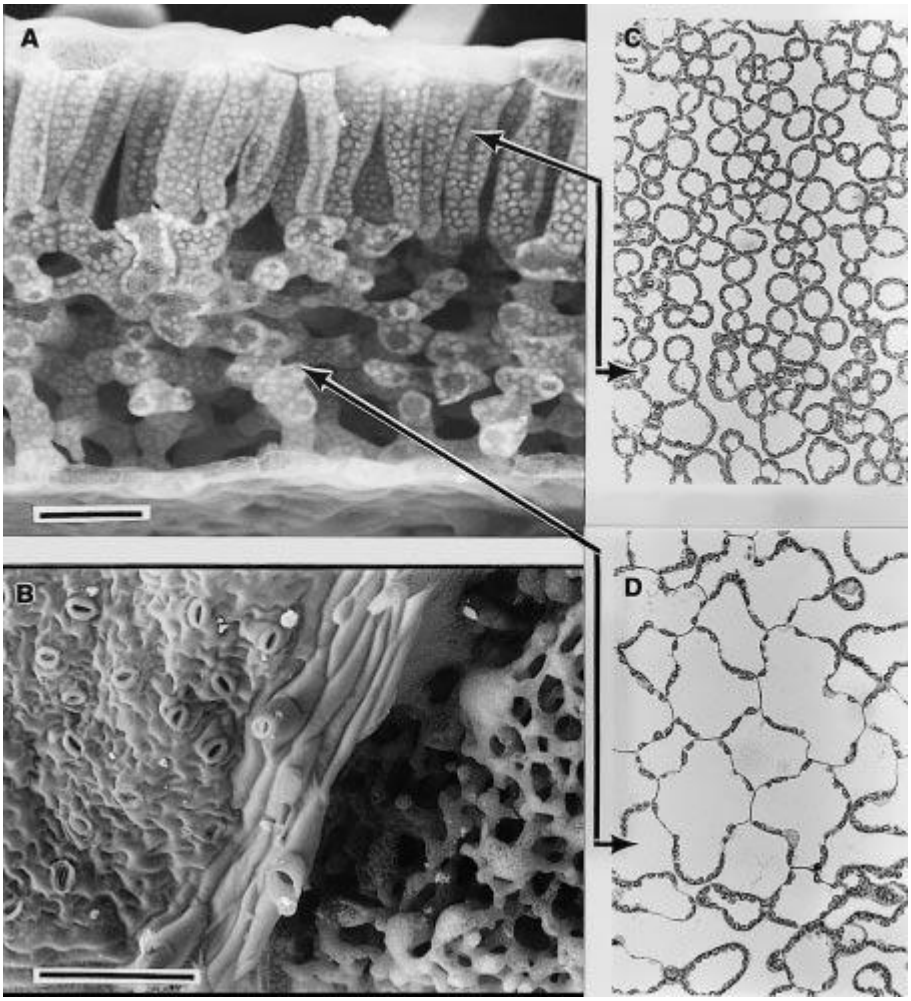

[4]

Figure 1.2 A scanning electron micrograph of an uncoated and rapidly frozen piece of tobacco leaf fractured in (A) to reveal palisade mesophyll cells beneath the upper leaf surface and spongy mesophyll in the lower half. Chloroplasts can be clearly seen covering the inner faces of cell walls. Looking onto the lower surface (B), the epidermis and stomata are present on the left side of the vein, whereas the epidermis was fractured away on the right side, revealing spongy mesophyll tissue. Light micrographs (C, D) of sections cut parallel to the leaf surface are shown for palisade (C) and spongy mesophyll (D) with solid lines showing where the paradermal sections align with (A). Chloroplasts form a dense single layer covering the cell surfaces exposed to intercellular airspace, but are rarely present lining walls where two cells meet. Scale bar in (A) = 50 µm and in (B) = 200 µm. Magnification given in (A) also applies to (C) and (D). (Original illustration from John Evans and Susanne von Caemmerer. See Evans et al. 1994 for related material)

1.1.2 Light absorption

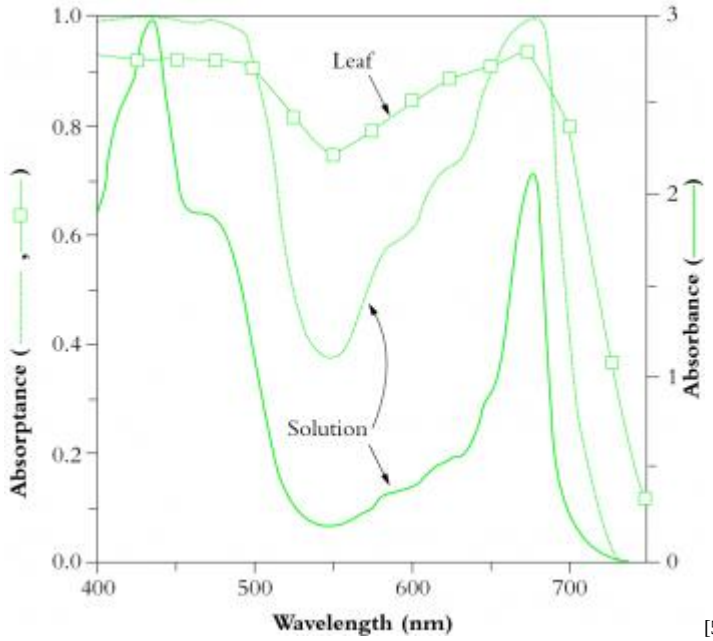

[5]

Figure 1.3 Light absorption by pigments in solution and by leaves. Absorbance (*A*) refers to attenuation of light transmitted through a leaf or a solution of leaf pigments, as measured in a spectrophotometer, and is derived from the expression $A = \log I_0/I$ where I_0 is incident light, and I is transmitted light. The solid curve (scale on right ordinate) shows absorbance of a solution of pigment—protein complexes equivalent to that of a leaf with 0.5 mmol Chl m^{-2}. The dotted curve shows *absorptance*(scale on left ordinate), and represents the fraction of light entering the solution that is absorbed. Virtually all light between 400 and 500 nm and around 675 nm is absorbed, compared with only 40% of light around 550 nm (green). The dashed curve with squares represents *leaf absorptance*, which does not reach 1 because the leaf surface reflects part of the incident light. Of light around 550 nm, 75% is absorbed because leaves scatter light effectively which increases the pathlength and thereby increases probability of absorption above that observed for the same pigment concentration in solution. (Based on McCree 1972; Evans and Anderson 1987)

Pigments in thylakoid membranes of individual chloroplasts (Figure 1.7) are ultimately responsible for strong absorption of wavelengths corresponding to blue and red regions of the visible spectrum (Figure 1.3). Irradiated with red or blue light, leaves appear dark due to this strong absorption, but in white light leaves appear green due to weak absorption around 550 nm, which corresponds to green light. Ultraviolet (UV) light (wavelengths below 400 nm) can be damaging to macromolecules, and sensitive photosynthetic membranes also suffer. Consequently, plants adapt by developing an effective sunscreen in their cuticular and epidermal layers.

Overall, absorption of visible light by mesophyll tissue is complex due to sieve-effects and scattering. Sieve-effect is an outcome from packaging pigments into discrete units, in this case chloroplasts, while remaining leaf tissue is transparent. This increases the probability that light can bypass some pigment and penetrate more deeply. A regular, parallel arrangement of palisade cells with chloroplasts all

vertically aligned means that about 80% of light entering a leaf initially bypasses the chloroplasts, and measurements of absorption in a light integrating sphere confirm this. Scattering occurs by reflection and refraction of light at cell walls due to the different refractive indices of air and water. Irregular-shaped cells in spongy tissues enhance scattering, increasing the path length of light travelling through a leaf and thus increasing the probability of absorption. Path lengthening is particularly important for those wavelengths more weakly absorbed and results in at least 80% absorption, even at 550 nm (Figure 1.3). Consequently, leaves typically absorb about 85% of incident light between 400 and 700 nm; only about 10% is reflected and the remaining 5% is transmitted. These percentages do of course vary according to genotype x environment factors, and especially adaptation to aridity and light climate.

Sunlight entering leaves is attenuated with depth in much the same way as light entering a canopy of leaves shows a logarithmic attenuation with depth that follows Beer's Law (Section 12.4). Within individual leaves, the pattern of light absorption is a function of both cell anatomy and distribution of pigments. An example of several spatial profiles for a spinach leaf is shown in Figure 1.4. Chlorophyll density peaks in the lower palisade layer and decreases towards each surface, declining exponentially with cumulative chlorophyll. Light absorption is then given by the product of the chlorophyll and light profiles. This increases from the upper surface, peaking near the base of the first palisade layer, then declines steadily towards the lower surface. Because light is the pre-eminent driving variable for photosynthesis, CO_2 fixation tends to follow the light absorption profile (see ^{14}C fixation pattern in Figure 1.4). However, the profile is skewed towards the lower surface because of a non-uniform distribution of photosynthetic capacity. Chloroplasts near the upper surface have 'sun'-type characteristics which include a higher ratio of Rubisco to chlorophyll and higher rate of electron transport per unit chlorophyll. Chloroplasts near the lower surface show the converse features of 'shade' chloroplasts. Similar differences between 'sun' and 'shade' leaves are also apparent. Chloroplast properties do not change as much as the rate of absorption of light. Consequently, the amount of CO_2 fixed per quanta absorbed increases with increasing depth beneath the upper leaf surface. The lower half of a leaf absorbs about 25% of incoming light, but is responsible for about 31% of a leaf's total CO_2assimilation.

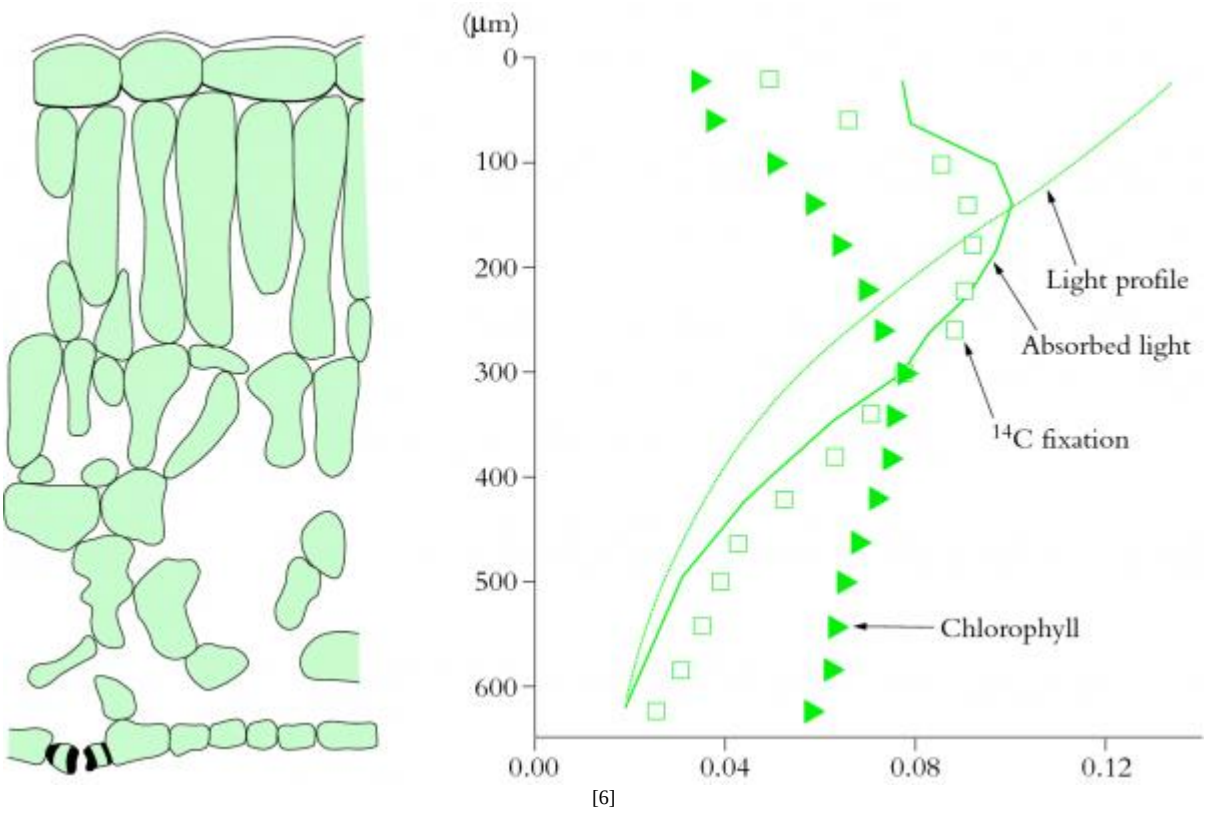

[6]

Figure 1.4 Profiles of chlorophyll, light absorption and photosynthetic activity through a spinach leaf. Cell outlines are shown in transverse section (left side).Triangles represent the fraction of total leaf chlorophyll in each layer. The light profile (dotted curve) can then be calculated from the Beer—Lambert law. The profile of absorbed light is thus the product of the chlorophyll and light profiles (solid curve). CO_2 fixation, revealed by ^{14}C labelling, follows the absorbed light profile, being skewed towards slightly greater depths. (Based on Nishio et el. 1993; Evans 1995)

1.1.3 CO2 diffusion to chloroplasts

Leaves are covered with a barrier or 'cuticle' on the outer walls of epidermal cells that is impermeable to both water and CO_2. Accordingly, CO_2 used in leaf photosynthesis gains entry via stomata (Figure 1.5), and as CO_2 molecules diffuse inwards they encounter an opposite flux of H_2O molecules rushing outwards that is three to four orders of magnitude stronger. Leaves control this gas exchange by adjusting the aperture of stomata which can vary within minutes in response to changes in several environmental variables including light, humidity and CO_2 concentration (see Chapter 15 for more details). Air-spaces inside leaves are effectively saturated with water vapour (equivalent to 100% relative humidity at that leaf temperature) and because air surrounding illuminated leaves is almost universally drier, water molecules diffuse in response to this concentration gradient from leaf to air.

The diffusion pathway for H_2O is usually divided into two parts, namely the boundary layer of still air at the leaf surface and stomatal pores (Figure 1.5).

Boundary layer thickness depends on windspeed, leaf dimensions and the presence of surface structures (e.g. hairs in Figure 1.1). Positioning of stomata also varies between species. Leaves of terrestrial plants always have stomata on their lower (abaxial) surface but many species have stomata on both surfaces, especially if they have high photosynthetic rates and are in sunny locations such as pendulant leaves of eucalypts. Adaptations for arid environments include having surface structures like hairs and waxes, which increase the thickness of the boundary layer, and leaf rolling and encryption of stomata by placing them in crevices in the leaf surface. While these features restrict water loss, they also impose an increased resistance (decreased conductance) to CO_2 uptake.

CO_2 molecules diffusing inwards from ambient air to chloroplasts encounter restrictions additional to boundary layer and stomata (Figure 1.5). CO_2 must also diffuse from substomatal cavities throughout the mesophyll, dissolve in wet cell walls, enter the cytosol across a plasmalemma, diffuse into chloroplasts across a double membrane (outer envelope in Figure 1.7) and finally reach fixation sites within the stroma of those chloroplasts.

There is considerable variation in leaf anatomy and hence potential restriction to CO_2 diffusion, but in general leaves with high rates of photosynthesis tend to have more permeable leaves (e.g. tobacco in Figure 1.2) and this complex anatomy ensures a greatly enlarged surface area for diffusion across interfaces. Indeed the total mesophyll cell wall area can be 20 times that of the projected leaf surface.

Diffusion to chloroplasts is further enhanced by their tendency to appress in clusters against cell walls adjacent to intercellular spaces (Figure 1.2 C, D), while carbonic anhydrase within chloroplasts speeds up diffusion of CO_2 by catalysing interconverion of CO_2 and bicarbonate within the stroma of chloroplasts. Although CO_2 rather than HCO_3^- is the substrate species for Rubisco, the presence of carbonic anhydrase enables bicarbonate ions, more abundant under the alkaline conditions (pH 8.0) that prevail inside chloroplasts, to diffuse to Rubisco in concert with diffusion of CO_2. By sustaining a very rapid equilibration between CO_2 and HCO_3^- immediately adjacent to active sites on Rubisco, carbonic anhydrase enhances inward diffusion of inorganic carbon.

1.1.4 Light and CO2 effects on leaf photosynthesis

Light impinging on plants arrives as discrete particles we term photons, so that a flux of photosynthetically active photons can be referred to as ‘photon irradiance’. A quantum (plural quanta) refers to a parcel of light energy carried by a photon, and is used here when referring to photosynthetic utilisation of energy derived from absorbed photons. Physicists recognise this subtle difference between

'photons' and 'quanta' and accord correct use. Plant biologists (incorrectly) use them interchangeably, a convention followed here.

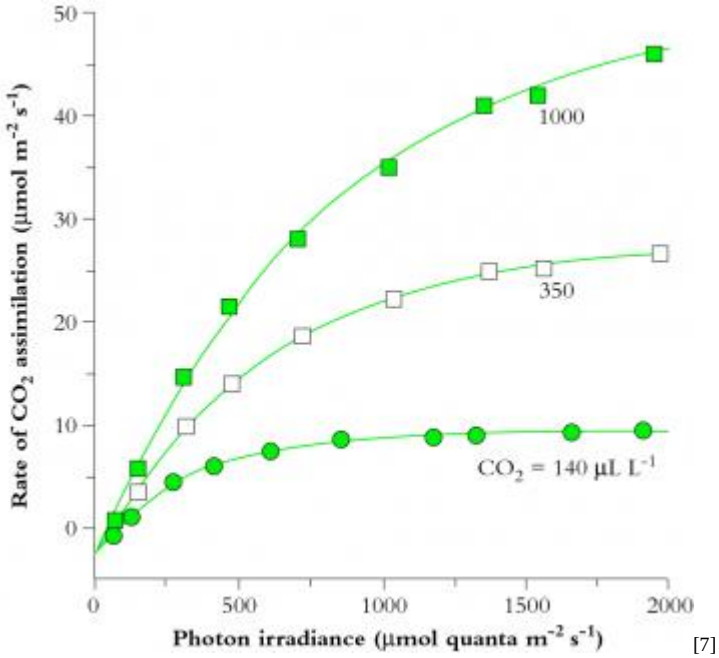

[7]

Figure 1.6 Photosynthetic response to photon irradiance for a *Eucalyptus maculata* leaf measured at three ambient CO_2concentrations, 140, 350 and 1000 µmol mol^{-1}. Irradiance is expressed as µmol quanta of photosynthetically active radiation absorbed, and net CO_2 assimilation is inferred from a drop in CO_2 concentration of gas passing over a leaf held in a temperature-controlled cuvette. CO_2 evolution in darkness is shown on the ordinate as an extrapolation below zero. The irradiance at which net CO_2 exchange is zero equals the light compensation point (commonly 15-50 µmol quanta m^{-2} s^{-1}, shade to sun species respectively). The initial slope of light-response curves for CO_2 assimilation per absorbed quanta represents maximum quantum yield for a leaf. (Based on Ögren and Evans 1993)

CO_2 assimilation varies according to both light and CO_2 partial pressure. At low light (low photon irradiance in Figure 1.6) assimilation rate increases linearly with increasing irradiance, and the slope of this initial response represents maximum quantum yield (mol CO_2 fixed per mol quanta absorbed). Reference to *absorbed* quanta in this expression is important. Leaves vary widely in surface characteristics (hence reflectance) as well as internal anatomy and chlorophyll concentration (chlorophyll content per unit mesophyll volume). Therefore absorption of photosynthetically active quanta will vary, so that quantum yield expressed in terms of incident irradiance can be misleading, and in the case of comparisons between sun and shade leaves has led to a widely held but mistaken belief that shade leaves (thinner and with higher chlorophyll concentration) are more efficient. Expressed in terms of absorbed quanta, sun and shade leaves have virtually identical quantum efficiencies for CO_2 assimilation.

Assimilation rate increases more slowly at higher irradiances until eventually a plateau is reached where further increases in irradiance do not increase the rate of

CO_2 assimilation (Figure 1.6). Chloroplasts are then light saturated. Absolute values for both quantum yield and light-saturated plateaux depend on CO_2 concentration. Quantum yield increases as CO_2 concentration increases because photorespiration is progressively suppressed. At ambient CO_2, photorespiration normally consumes about one-third of available photochemical energy. The quantum yield for incident light also depends primarily on chlorophyll content. Leaf absorptance has a hyperbolic dependence on chlorophyll content. For most leaves, 80–85% of 400–700 nm light is absorbed and it is only in leaves produced under severe nitrogen deficiency where there is less than 0.25 mmol Chl m^{-2} that absorptance falls below 75%.

The plateau in Figure 1.6 at high irradiance is set by maximum Rubisco activity. With increasing CO_2 partial pressure, the rate of carboxylation increases along with a reduction in photorespiration. Note, however, that the transition from light-limited to Rubisco-limited CO_2 assimilation as irradiance increases is not a classic Blackman curve (i.e. with a sharp transition), and becomes progressively more gradual at higher CO_2partial pressures. In part, this gentle transition reflects the fact that a leaf is a population of chloroplasts which have different photosynthetic properties depending on their position within that leaf. As discussed above, the profile of photosynthetic capacity per chloroplast changes less than the profile of light absorption per chloroplast (Figure 1.4). This results in an increase in CO_2 fixed per quanta absorbed with increasing depth. A transition from a light to a Rubisco limitation therefore occurs at progressively higher incident irradiances for each subsequent layer and results in a more gradual transition in the irradiance response curve of a leaf compared to that of a chloroplast.

Photosynthetic capacity of leaves varies widely according to light, water and nutrient availability and these differences in capacity usually reflect Rubisco content. Leaves in high light environments (‘sun’ leaves) have greater CO_2 assimilation capacities than those in shaded environments and this is reflected in the larger allocation of nitrogen-based resources to photosynthetic carbon reduction (PCR cycle; Section 2.1). Sun leaves have a high stomatal density, are thicker and have a higher ratio of Rubisco to chlorophyll in order to utilise the larger availability of photons (and hence ATP and NADPH). Shade leaves are larger and thinner, but have more chlorophyll per unit leaf dry weight than sun leaves. They can have a greater quantum yield per unit of carbon invested in leaves, but with a relatively greater allocation of nitrogen-based resources to photon capture, shade leaves achieve a lower maximum rate of assimilation.

Despite such differences in leaf anatomy and chloroplast composition, leaves sustain energy transduction and CO_2 fixation in an efficient and closely coordinated fashion. Processes responsible are discussed below (Section 1.2).

CASE STUDY 1.1 Development of A:pi curves

Susanne von Caemmerer and Graham Farquhar

Component processes underlying CO_2 assimilation are amenable to analysis at a whole-leaf level. Under strong illumination, CO_2-assimilation clearly predominates over CO_2-generating processes (both mitochondrial and photorespiration), and in those circumstances the inward flux of CO_2 can be taken as a net reaction rate for CO_2 assimilation via Rubisco as primary catalyst. However, if whole-leaf photosynthesis is to be analysed in biochemical terms, the effective concentration of this primary substrate at fixation sites must also be known. How then can these substrate levels be defined in an actively photosynthesising leaf? Moreover, knowing that CO_2 assimilation is energy dependent, and that both ATP and reducing power (NADPH) are being generated concurrently, how can photosynthetic electron flow be described in terms relevant to CO_2 assimilation?

Early models of leaf gas exchange had been developed as electrical analogues of resistances, and proved useful in making a distinction between stomatal and mesophyll limitations on CO_2 assimilation. Mesophyll, or 'residual', resistance (r_{mc}) was a collective term that was meant to embody non-stomatal diffusive factors, and included both physical and biochemical constraints. Further refinement would depend upon a reliable estimate of CO_2 partial pressure at fixation sites within leaves, and those estimates came with improvements in diffusive models for leaves, but, in particular, development of high- precision gas exchange systems with a capacity for fast data analysis (either by interfacing measuring devices with computers, or via chart recorder and human agency!). CO_2 response curves emerged as a valuable tool to analyse photo-synthesis *in vivo*.

In this essay A:c_i refers to CO_2 assimilation rate (A) as a function of intercellular CO_2 concentration (c_i) expressed in terms of µL of CO_2 per litre of gas (µL L^{-1}) or µg of CO_2 per litre of gas (µg L^{-1}). In strict biophysical terms, intercellular CO_2 partial pressure (p_i) rather than gaseous concentration (c_i) is a more relevant determinant of CO_2 assimilation, and where leaf chamber atmospheric pressure is known, an A:p_i curve can be constructed. CO_2 assimilation rate (A) is then referenced to intercellular partial pressure (p_i) expressed as µbar where p_i = chamber pressure × c_i. At one bar atmospheric pressure, p_i is numerically equivalent to c_i.

Physical concepts of leaf gas exchange

Penman and Schofield (1951) put diffusion of CO_2 and water vapour through stomata on a firm physical basis. Their ideas were taken up at Wageningen by

Pieter Gaastra in the 1950s and modern analytical gas exchange is often attributed to this seminal work (Gaastra 1959) where he even constructed his own infrared gas analyser and other equipment necessary to make measurements of CO_2 and water vapour exchange. His work was a landmark because it examined CO_2 assimilation and water vapour exchange rates of individual leaves under different environmental conditions, and he distinguished between stomatal and internal resistances. Gaastra calculated resistances to water vapour and CO_2 diffusion from two equations (here in our simplified notation) which are based on Fick's Law for the diffusion of gases.

$$E = \frac{w_i - w_a}{r_s w} \text{ and } A = \frac{c_a - c_i}{r_s c} \qquad (1)$$

where E and A are the fluxes of water vapour and CO_2 and w_i and c_i and w_a and c_a are the mole fractions of water vapour and CO_2 in intercellular air spaces and ambient air respectively. The denominator terms, r_{sw} and r_{sc}, represent stomatal resistances to H_2O and CO_2 diffusion respectively. Gaastra calculated w_i from the saturated vapour pressure at the measured leaf temperature and since both E and $w_a$were measured variables this allowed r_{sw} to be calculated. Knowing that resistances to CO_2 and water vapour are related by the ratio of their diffusivities, he calculated stomatal resistance to CO_2 diffusion, r_{sc}. Gaastra realised that the diffusion path for CO_2 is longer than that of water vapour, as CO_2 had to diffuse from the intercellular airspaces through the cell wall across membranes to the chloroplast stroma where CO_2 fixation by Rubisco takes place. He therefore extended the equation for CO_2 assimilation to:

$$A = \frac{c_a - c_{chl}}{r_{sc} + r_{mc}} \qquad (2)$$

where c_{chl} represented CO_2 concentration at chloroplasts.

Gaastra analysed the dependence of CO_2 assimilation rate on light, CO_2 and temperature, and observed that at low CO_2 concentrations the rate of CO_2 assimilation was independent of temperature whereas it was strongly influenced by temperature at higher CO_2. This led him to conclude that the rate of CO_2 uptake was completely limited by CO_2 diffusion processes at low CO_2 and that biochemical processes became limiting only at high CO_2. The belief that CO_2 diffusion was limiting gave rise to the assumption that chloroplastic CO_2 concentration was close to zero. This led to the erroneous simplification of the above equation such that the total resistance to CO_2 diffusion could be calculated from CO_2 assimilation rate and the ambient CO_2 concentration alone. Since stomatal resistances could be calculated from measurements of water vapour diffusion, it was also possible to calculate mesophyll resistance to CO_2 diffusion. In Australia particularly there was a great interest in determining the relative

importance of stomatal and mesophyll resistance in limiting CO_2 assimilation rates under adverse conditions of high temperature and frequent water stresses, and in global terms much of the pioneering work was undertaken in this country (see, for example, Bierhuizen and Slatyer 1964).

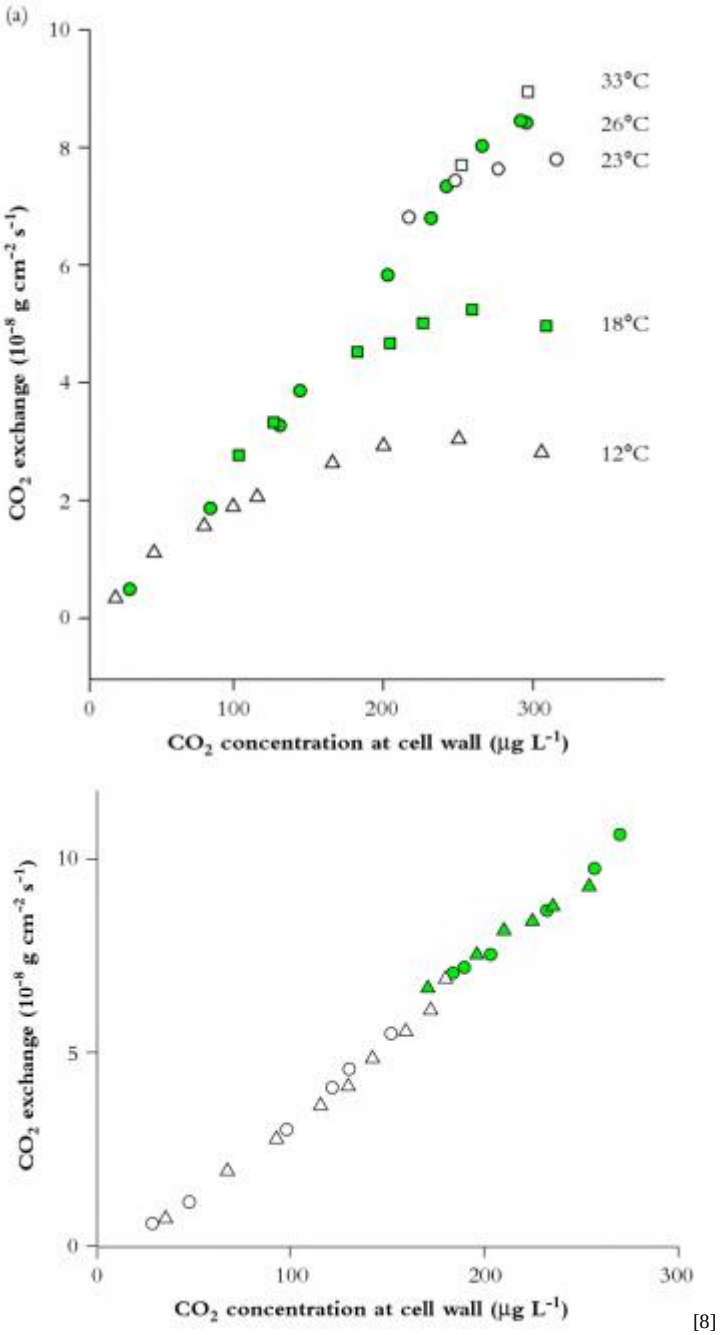

[8]

Figure 1 An early A:c_i curve showing the CO_2 assimilation rate of cotton at a range of cell wall CO_2 concentrations (redrawn from Troughton (1969) and Troughton and Slayter (1969) and retaining original units for CO_2 flux). For comparative purposes, 10×10^{-8} g cm^{-2} s^{-1} would be equivalent to 22.27 µmol CO_2 m^{-2} s^{-1}, and 1 µg L^{-1} would be equivalent to 0.54 µL L^{-1}(assuming a gram molecular weight of 44 for CO_2, and measurements at normal temperature and pressure). (a) Leaf temperature influences the overall shape of CO_2 response curves (measured in O_2-free air) but has no effect on the initial slope where response to CO_2 is limited by Rubisco activity.

This family of curves comes from repeated measurements of gas exchange by the same leaf at five different temperatures (values shown) and indicated in the figure by five different symbols. (b) CO_2 response curves for two leaves of cotton measured in O_2-free air at 25°C and three levels of relative water content. Legend: ● leaf 1, 92% water content; O leaf 1, 56%; ▲ leaf 2, 92%; △ leaf 2, 69%. Identical slopes regardless of treatment mean that variation in relative water content over this range is without effect on CO_2 assimilation within mesophyll tissues. By implication, reduction in CO_2 uptake as commonly observed on whole leaves under moisture stress would be attributable to stomatal factors.

Calculation of intercellular CO_2, c_i and the first A versus c_i curves

Although CO_2 concentration in intercellular airspaces, c_i, was explicit in Gaastra's equations, this term was first specifically calculated by Moss and Rawlings in 1963, and the first extensive use of the parameter was made by Whiteman and Koller in 1967, who examined stomatal responses to CO_2 and irradiance, concluding that stomata were more likely to respond to c_i rather than c_a. The first *bona fide* response curves of CO_2 assimilation rate to c_i rather than c_a were those of Troughton (1969) and Troughton and Slatyer (1969) (Figure 1). In Figure 1(a), c_i was derived from measurements of CO_2 uptake in an assimilation chamber where air passed through a leaf, rather than over both surfaces concurrently (as became commonplace in subsequent designs), and such estimates would differ slightly. More importantly, those measurements were made at different temperatures and confirmed that CO_2 assimilation was not greatly affected by temperature at low c_i. Later, this lack of temperature dependence was explained by the kinetics of Rubisco (von Caemmerer and Farquhar 1981). Figure 1(b) shows the initial slope of CO_2 response curves measured at different stages of water stress. In this case, water stress has affected stomatal resistance (as the c_i obtained at air levels of CO_2 occur at progressively lower c_i) but not the relationship between CO_2 assimilation rate and c_i. A versus c_i response curves thus provided an unambiguous distinction between stomatal and non-stomatal effects on CO_2 assimilation and, provided stomata respond uniformly across both leaf surfaces, that distinction can be made quantitative.

Before we head further into a discussion of our 1990s understanding and interpretation of more comprehensive CO_2 response curves, we must take an important digression into development of mathematical models of C_3 photosynthesis.

Biochemistry of photosynthesis and leaf models

Gas exchange studies focused initially on physical limitations to diffusion, but it was not long before persuasive arguments were being brought forward to show that leaf biochemistry must influence the rate of CO_2 fixation even at low CO_2 concentrations. Björkman and Holmgren (1963) made careful gas exchange measurements of sun and shade ecotypes of *Solidago* growing in Sweden, and

noted strong correlations between photosynthetic rate measured at high irradiance and ambient CO_2 and the nitrogen content of leaves, and later also related it to different concentrations of Rubisco (then called carboxydismutase). Anatomical studies implied that thin shade leaves would not have larger internal diffusion resistance to CO_2 than thicker sun leaves where cells were more densely packed. Furthermore, following earlier discoveries of the O_2sensitivity of photosynthesis, namely a low-O_2 enhancement of CO_2 assimilation rate, Gauhl and Björkman (1969), then at Stanford, showed very elegantly that while O_2 concentration did affect CO_2 assimilation rate, water vapour exchange was not affected (i.e. stomata had not responded). Clearly, the increase in CO_2 assimilation rates seen with a decrease in O_2 concentration could not be explained via a limitation on CO_2 diffusion.

Central importance of Rubisco

Early mathematical models of leaf photosynthesis were extensions of Gaastra's resistance equation, and could not accommodate the O_2sensitivity of CO_2 assimilation. They were quickly followed by development of more biochemical models in the early 1970s and the discoveries by Bowes *et al*. (1971) that Rubisco was responsible for both carboxylation and oxygenation of RuBP (a five-carbon phosphorylated sugar, regenerated by the PCR cycle of chloroplasts). This crucial observation of dual function put Rubisco at centre stage. Laing *et al.* (1974) were first to compare the gas exchange of soybean leaves with the *in vitro* kinetics of Rubisco and suggested the following equation for the net CO_2assimilation rate:

$$A = V_c\left(1 - 0.5\frac{V_o}{V_c}\right) \qquad (3)$$

where V_c and V_o are the rates of Rubisco carboxylation and oxygenation (later on a term for mitochondrial respiration was added to most models). Laing *et al*. related a ratio of the rates of carboxylation to oxygenation of RuBP to the con-centration of its substrates, CO_2, C, and O_2, O, and showed that:

$$\frac{V_o}{V_c} = \frac{V_{omax}K_c}{V_{cmax}K_o}\frac{O}{C} = 2\Gamma\star/C \qquad (4)$$

where K_c, K_o, V_{cmax}, V_{omax} are the corresponding Michaelis Menten constants and maximal activities of carboxylase and oxygenase functions respectively and $\Gamma*$ is the CO_2 compensation point in the absence of mitochondrial respiration.

A note on Γ: illuminated leaves held in a closed circuit of recirculating air will reduce CO_2 to a 'compensation point' where uptake and generation of CO_2 are balanced; this is commonly 50–100 ppm for C_3 plants and referred to as Γ. A

CO_2 response curve for leaf photosynthesis will show a similar value as an intercept on the abscissa. Γ can thus be measured empirically, and will be an outcome of interactions between photosynthesis, photorespiration and dark (mitochondrial) respiration (R_d). If allowance is made for R_d, the CO_2 compensation point would then be slightly lower, and is termed Γ∗. As with measured Γ, this inferred CO_2 compensation point, Γ∗, is linearly related to O_2, an observation that intrigued earlier observers but was easily reconciled with the dual function of Rubisco. Laing *et al*. (1974) used Equations 3 and 4 to predict this linear dependence of Γ∗ on O_2, and with subsequent confirmation Rubisco became a key player in photosynthetic models. (Equation 3 assumes that for each oxygenation, 0.5 CO_2 are evolved in the subsequent photorespiratory cycle, although there has been some debate over this stoichiometry.) If the enzyme reaction is ordered with RuBP binding first, the rate of carboxylation in the presence of the competitive inhibition by O_2 at saturating RuBP concentration can be given by

$$V_c = \frac{CV_{max}}{C + K_c(1 + O/K_o)} \qquad (5)$$

When combined with Equation 3 this gave a simple expression of net CO_2 fixation rate:

$$A = \frac{(c_i - \Gamma\star)V_{cmax}}{(c_i + K_c(1 + O/K_o))} \qquad (6)$$

which depends on the maximal Rubisco activity and provided the quantitative framework for comparing rates of CO_2 assimilations with the amount of Rubisco present in leaves (von Caemmerer and Farquhar 1981). Difference in CO_2 assimilation rates observed under different growth con-ditions could then be explained according to variations in the amount of Rubisco present in leaves. In Figure 2 the dotted line shows a CO_2 response curve modelled by Equation 6. Chloroplast CO_2 partial pressure was then assumed to be similar to that in the intercellular airspaces. Using on-line discrimination between $^{13}CO_2$ and $^{12}CO_2$, and deriving an estimate of CO_2 partial pressure at fixation sites within chloroplasts, we subsequently learned that a further draw down can occur, but the general applicability of Equation 6 was not compromised. As an aside, these equations became basic to most photosynthetic models long before the order of the reaction mechanism of Rubisco had been unequivocally established. Had CO_2 and O_2 bound to Rubisco before RuBP, or the reaction not been ordered, our equations would have been much more complex with both $K_m(CO_2)$ and $K_m(O_2)$ dependent upon RuBP concentration.

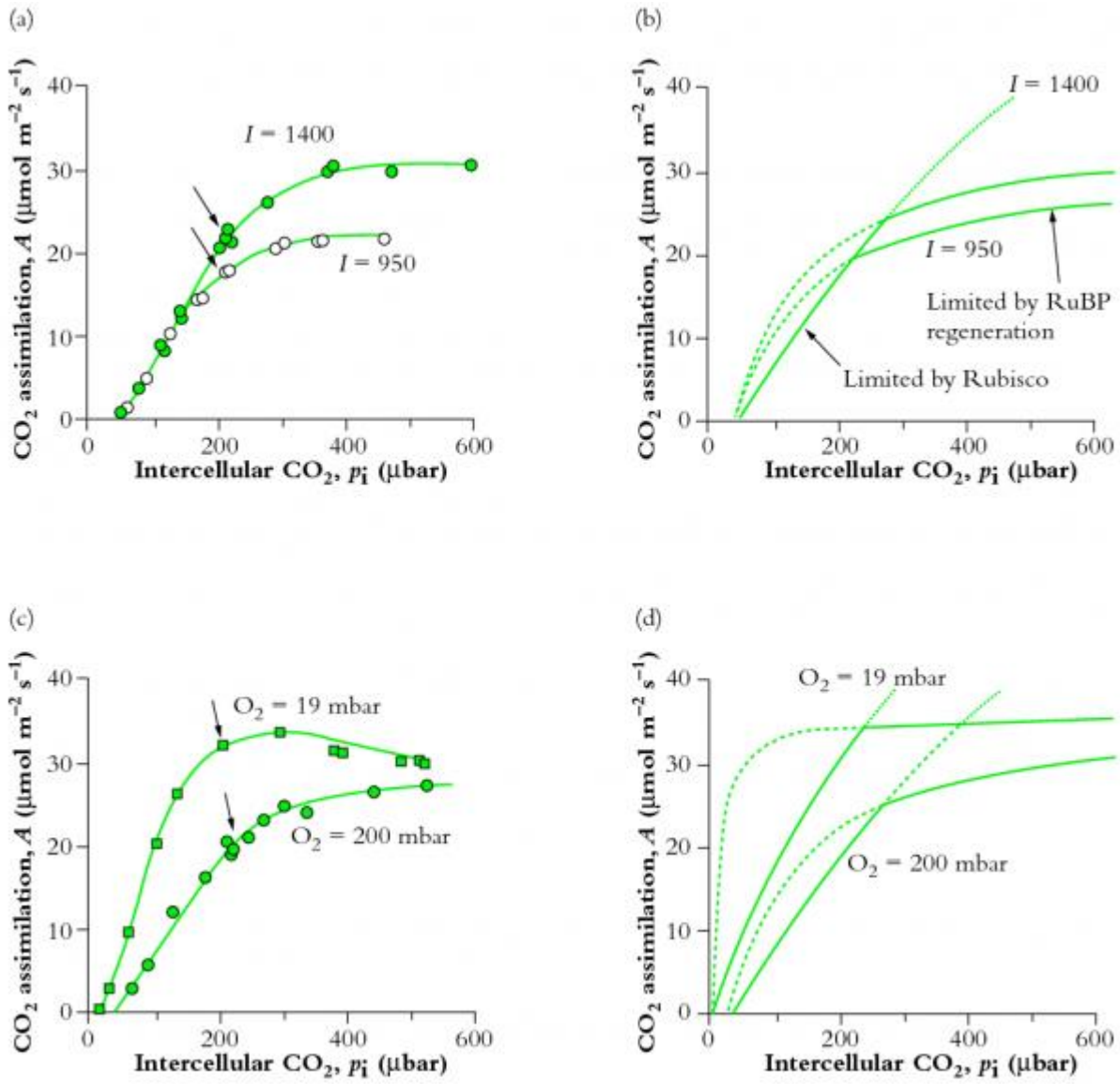

[9]

Figure 2 Comparison of measured and modelled CO_2 response curves. (a) CO_2 assimilation rate v. intercellular CO_2 partial pressure in Phaseolus vulgaris measured at two irradiances and a leaf temperature of 28°C. Arrows indicate points obtained at an external CO_2 partial pressure of 330 µbar. (b) Modelled CO_2response curves. The dotted line and its extension represent the Rubisco-limited rate of CO_2 assimilation $\left(A = \frac{(c_i-\Gamma_\star)V_{cmax}}{c_i+K_c(1+O/K_c)} - R_d\right)$. The dashed lines and their extensions represent the electron-transport-limited rates of CO_2 assimilation at the two irradiances $\left(A = \frac{(c_i-\Gamma_\star)J}{4.5c_i+10.3\Gamma\star} - R_d\right)$. For further details see von Caemmerer and Farquhar (1981). (c) CO_2 assimilation rate v. intercellular CO_2concentration in Phaseolus vulgaris measured at two O_2 concentrations at a leaf temperature of 28°C. Arrows indicate points obtained at an external CO_2 partial pressure of 330 µbar. (d) Modelled CO_2 response curves for conditions applied in (c). (Method details in (b)) .

Regeneration of RuBP and electron transport rate

Equation 6 could mimic CO_2 assimilation rate at low c_i , as well as O_2 effects on CO_2 uptake, but measured rates of CO_2 assimilation saturated much more abruptly at high CO_2 concentrations than could be predicted from Rubisco kinetics (Figure 2). Using a highly novel approach in Estonia, Laisk and Oja (1974) proposed that CO_2 assimilation was limited by RuBP regeneration rate at high c_i. They had fed brief pulses of CO_2 to leaves that had been previously exposed to low CO_2 (conditions under which RuBP concentrations were presumably high), and obtained rates up to 10 times higher than the steady-state rates of CO_2 assimilation! Lilley and Walker (1975) at Sheffield reached a similar conclusion after comparing the CO_2 responses of illuminated isolated chloroplasts with those obtained upon lysing chloroplasts in a medium containing saturating RuBP.

In our model of C_3 photosynthesis (Farquhar *et al*. 1980) the way we handled rate limitation by RuBP regeneration was probably the most important decision made in that context. Both ATP and NADPH were required for RuBP regeneration, and this fundamental need formed a connection with light in our model. From a mathematical perspective there were two options: (1) RuBP and CO_2 could always colimit the rate of carboxylation, and this we would express in a double Michaelis Menten equation, or (2) carboxylation rate could be limited by either RuBP or else saturated and thus independent of RuBP. The *in vivo* kinetics of Rubisco suggest the second option.

Peisker (1974) and Farquhar (1979) pointed out that Rubisco was unusual in that it was present in the chloroplast at very high concentrations. Given such a low K_m(RuBP), this meant that the *in vivo*kinetics with respect to chloroplastic RuBP were those of a tight binding substrate. That is, the rate of Rubisco would depend linearly on RuBP concentration when chloroplastic RuBP concentration was below Rubisco catalytic site concentration, and once RuBP exceeded Rubisco site concentration carboxylase would be RuBP saturated. We also knew that irradiance affected CO_2 assimilation rate mainly at high intercellular CO_2. This supported option 2 (see Figure 2a, b). Given these insights, the more complex link between chloroplastic electron transport rate and RuBP pools used by Farquhar *et al*. (1980) was quickly simplified to a description of CO_2 assimilation that was limited by RuBP regeneration, and utilisation of ATP and NADPH for photosynthetic carbon reduction or oxygenation. RuBP regeneration was in turn driven by the electron transport rate, *J* (dependent on irradiance and its own maximal capacity), and stoichiometry of ATP or NADPH use by the photosynthetic carbon reduction and oxygenation cycle. For example, when electron transport rate, *J*, was limiting (in view of ATP use) carboxylation rate could proceed at:

$$V_c = J/(4.5 + 10.5\Gamma\star/C) \qquad (7)$$

Dashed lines in Figure 2 give modelled electron-transport-limited rates of CO_2 fixation according to:

$$A = \frac{J(c_i - \Gamma\star)}{4.5c_i + 10.5\Gamma\star} \qquad (8)$$

This simplified formulation of C_3 photosynthesis (Equations 6 and 8) now provides a meaningful framework for analysis of leaf photosynthesis, and has focused our interpretation of CO_2 response curves on leaf biochemistry. For example, von Caemmerer and Farquhar (1981) related the initial slopes of CO_2 response curves to *in vitro* Rubisco activity, and the CO_2-saturated rates of A:c_i curves to *in vitro*measurements of electron transport rates. Such studies validate Equations 6 and 8, demonstrating that CO_2 response curves could be used as a meaningful and non-invasive tool to quantify these biochemical components under a wide variety of conditions. Subsequent comparisons between wild-type tobacco and transgenic tobacco with a reduced amount of Rubisco have confirmed our concepts. When Rubisco alone is reduced in transgenic plants, RuBP regeneration capacity remains unchanged and no longer limits the rate of CO_2 assimilation at high CO_2. Rubisco then constitutes the sole limitation (Figure 3).

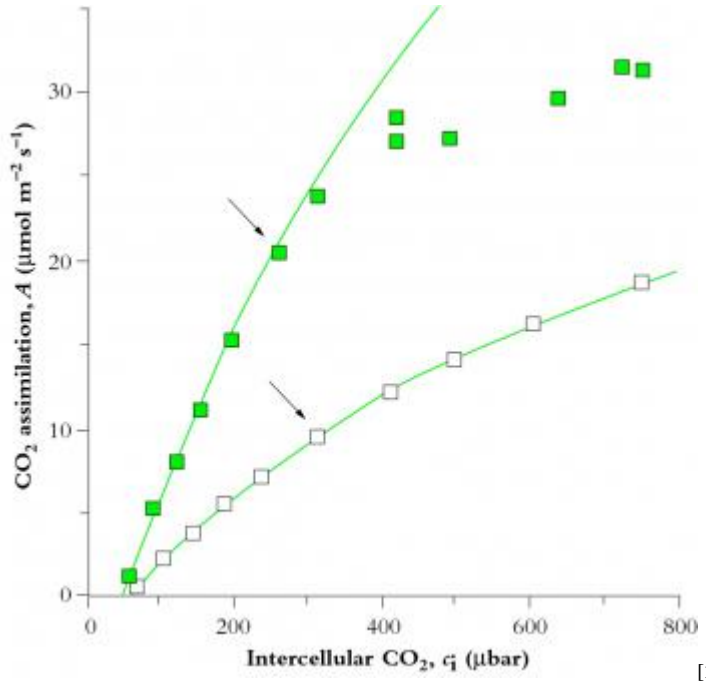

[10]

Figure 3 Transgenic tobacco with reduced amount of Rubisco shows no limitation by the rate of RuBP regeneration. CO_2assimilation response curves in wild-type tobacco, ■, and in transgenic tobacco with reduced amount of Rubisco, □, were measured at a photon irradiance of 1000 µmol quanta m^{-2} $s^{-1}$and a leaf temperature of 25°C. Lines show Rubisco-limited rates of CO^2 assimilation (see legend to Figure 2).The reduction in Rubisco in transgenic tobacco was achieved with an antisense gene directed against the mRNA of the Rubisco small subunit (Hudson et al. 1992). Arrows indicate the points obtained at an external CO_2 partial pressure of 350 µbar .

Colimitation

Both Rubisco and electron transport components are expensive in terms of leaf nitrogen. For example, Rubisco represents up to 25% of a leaf's protein nitrogen, with energy transduction components a further 25%. At a c_i where the transition from a Rubisco limitation to RuBP regeneration limitation occurs, both capacities are used efficiently and colimit net CO_2 assimilation. That is, assimilation can only be increased if both sets of component processes are increased. Where then should the balance lie if a plant is to use nitrogen-based resources to best effect? The transition obviously varies with irradiance and temperature so that an optimal balance will vary with habitat. However, surprisingly little variation has been observed and plants appear unable to shift this point of balance. As an example, important in the context of rising atmospheric CO_2 concentrations, plants grown in a high CO_2 environment should manage with less Rubisco and thus put more nitrogen into the capacity of RuBP regeneration. Surprisingly, such adjustments have not been observed experimentally, but given prospects of global change, our need for understanding gains urgency.

References

Bierhuizen, J.F. and Slatyer, R.O. (1964). 'Photosynthesis of cotton leaves under a range of environmental conditions in relation to internal and external diffusive resistances', *Australian Journal of Biological Sciences*, **17**, 348–359.

Björkman, O. and Holmgren, P. (1963). 'Adaptability of the photosynthetic apparatus to light intensity in ecotypes from exposed and shaded habitats', *Physiologia Plantarum*, **16**, 889–914.

Bowes, G., Ogren, W.L. and Hageman, R.H. (1971). 'Phosphoglycolate production catalysed by ribulose diphosphate carboxylase', *Biochemical and Biophysical Research Communications*, **45**, 716–722.

Evans, J.R. and von Caemmerer, S. (1996). 'CO_2 diffusion inside leaves', *Plant Physiology*, **110**, 339–346.

Farquhar, G.D. (1979). 'Models describing the kinetics of ribulose bisphoshate carboxylase–oxygenase', *Archives of Biochemistry and Biophysics*, **193**, 456–468.

Farquhar, G.D., von Caemmerer, S. and Berry, J.A. (1980). 'A biochemical model of photosynthetic CO_2 assimilation in leaves of C_3 species', *Planta*, **149**, 78–90.

Gaastra, P. (1959). 'Photosynthesis of crop plants as influenced by light, carbon dioxide, temperature and stomatal diffusion resistance', *Mededelingen Landbouwhogeschool Wageningen*,
59, 1–68.

Gauhl, E. and Björkman, O. (1969). 'Simultaneous measurements on the effect of oxygen concentration on water vapor and carbon dioxide exchange', *Planta*, **88**, 187–191.

Hudson, G.S., Evans, J.R., von Caemmerer, S., Arvidsson, Y.B.C. and Andrews, T.J. (1992). 'Reduction of ribulose-1,5-bisphosphate carboxylase/oxygenase content by antisense RNA reduced photosynthesis in tobacco plants', *Plant Physiology*, **98**, 294–302.

Laing, W.A., Ogren, W. and Hageman, R. (1974). 'Regulation of soybean net photosynthetic CO_2 fixation by the interaction of CO_2, O_2 and ribulose-1,5-diphosphate carboxylase', *Plant Physiology*, **54**, 678–685.

Laisk, A. and Oja, V.M. (1974). 'Photosynthesis of leaves subjected to brief impulses of CO_2', *Soviet Journal of Plant Physiology*, **21**, 928–935.

Lilley, R. McC. and Walker, D.A. (1975). 'Carbon dioxide assimilation by leaves, isolated chloroplasts and ribulose bisphosphate carboxylase from spinach', *Plant Physiology*, **55**, 1087–1092.

Moss, D.N. and Rawlings, S.L. (1963). 'Concentration of carbon dioxide inside leaves', *Nature*, **197**, 1320–1321.

Peisker, M. (1974). 'A model describing the influence of oxygen on photosynthetic carboxylation', *Photosynthetica*, **8**(1), 47–50.

Penman, H.J. and Schofield, R.K. (1951). 'Some physical aspects of assimilation and transpiration', *Symposium of the Society of Experimental Biology*, **5**, 115–129.

von Caemmerer, S. and Farquhar, G.D. (1981). 'Some relationships between the biochemistry of photosynthesis and the gas exchange of leaves', *Planta*, **153**, 376-387.

Troughton, J.H. (1969). Regulation of carbon dioxide exchange in plants, PhD thesis, Australian National University, Canberra.

Troughton, J.H. and Slatyer, R.O. (1969). 'Plant water status, leaf temperature and the calculated mesophyll resistance to carbon dioxide of cotton', *Australian Journal of Biological Sciences*, **22**, 815–827.

Whiteman, P.C. and Koller, D. (1967). 'Interactions of carbon dioxide concentration, light intensitiy and temperature on plant resistance to water vapour and carbon dioxide diffusion', *New Phytologist*, **66**, 463–473.

1.2 Chloroplasts and energy capture

In thermodynamic terms, O_2-generating photosynthesis in vascular plants is an improbable process! Improbable, because a weak oxidant (CO_2) must oxidise a weak reductant (H_2O), thereby producing a strong oxidant (O_2) and a strong reductant (carbohydrate). To achieve this 'uphill' reaction, a massive and continuous input of chemical energy is required. However, in nature, only radiant energy is available on that scale. How then can green plants achieve this conversion? Chloroplasts are responsible, and in what is unarguably the most significant process in our biosphere, photosynthetically active quanta are trapped and converted into chemically usable forms. This captured energy sustains plant growth and provides a renewable resource base for life on earth.

Thanks to the pioneering work of Calvin and Benson at Berkeley on $^{14}CO_2$ fixation products by *Chlorella* which began in the 1950s, biochemical aspects of photosynthetic carbon reduction (Calvin cycle) are now comprehensively understood. Not so energy transduction, and while events surrounding photosynthetic electron flow are defined in some detail and are described here, biophysical processes within the water-splitting apparatus of chloroplasts, and indeed the manner in which photons are captured and their quantum energy harnessed for photolysis, remain something of an enigma and fall outside the scope of our present account.

1.2.1 Chloroplast structure and composition

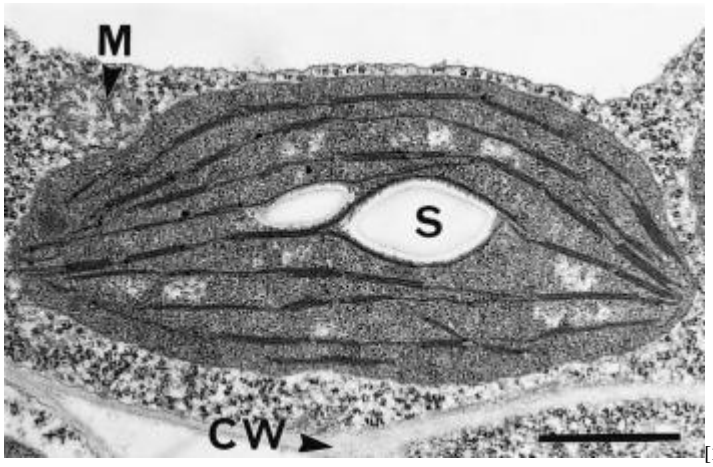

[11]

Figure 1.7 A mature and functional chloroplast in an immature leaf of bean (*Phaseolus vulgaris*) with an extensive network of photosynthetic membranes (thylakoids), parts of which are appressed into moderate granal stacks, and suspended in a gel-like matrix (stroma).The chloroplast contains a pair of starch grains (S) encapsulated in a double membrane (envelope) and suspended within a granular cytoplasmic matrix adjacent to a mitochondrion (M) and in close proximity to the cell wall (CW). Scale bar = 1 µm . (Transmission electron micrograph courtesy Stuart Craig and Celia Miller, CSIRO Plant lndustry, Canberra)

Chloroplasts are easily recognised under a light microscope in leaf sections as distinctive green organelles suspended in the cytoplasm and usually appressed against cell walls. Chloroplasts are abundant in mesophyll tissue (commonly 200–300 in each palisade cell) and functional organelles can be isolated from homogenates of leaf tissue.

Chloroplasts are surrounded by a double membrane, or envelope, just visible in transmission electron micrographs (Figure 1.7). This envelope encapsulates a soluble (gel-like) stroma which contains all the enzymes necessary for carbon fixation, many enzymes of nitrogen and sulphur metabolism and the chloroplast's own genetic machinery.

The inner membrane of a chloroplast envelope is an effective barrier between stroma and cytoplasm, and houses transporters for phosphate and metabolites (Section 2.1.8) as well as some of the enzymes for lipid synthesis. By comparison, the outer membrane of the chloroplast envelope is less complex and more permeable to both ions and metabolites.

Suspended within the stroma, and entirely separate from envelope membranes, is an elaborately folded system of photosynthetic membranes or 'thylakoids' (literally 'little sacs'). Embedded within these membranes are large populations of four basic complexes comprising two types of photosystem (with interlinked protein and pigment molecules), cytochrome *b*/*f* complexes (pivotal for photosynthetic electron transport) and ATP synthase complexes (responsible for proton egress from thylakoid lumen to stroma, and consequent ATP generation). Collectively, these complexes enable light harvesting and electron flow from H_2O molecules to $NADP^+$, thereby converting solar energy into chemically usable forms. This remarkable conversion, with such profound implications for life as we know it, starts with selective absorption of incoming light by chlorophylls and accessory pigments (certain carotenoids) that operate within both photosystems.

1.2.2 Chlorophyll absorption and photosynthetic action spectra

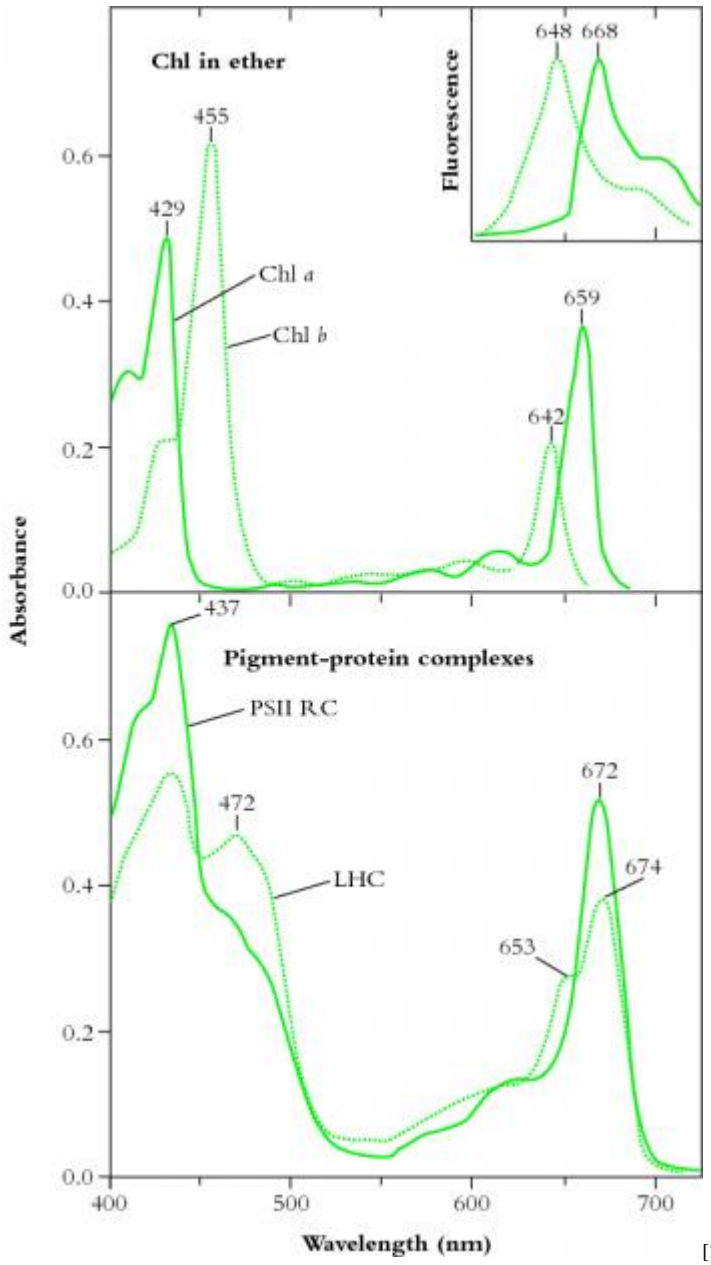

[12]

Figure 1.8 Upper curves: Diethylether solutions of chlorophyll *a*(Chl *a*, solid line) and chlorophyll *b* (Chl *b*, dotted line) show distinct absorption peaks in blue and in red regions of the visible spectrum (redrawn from Zscheile and Comar's (1941) original data). Fluorescence emission spectra (inset, redrawn from Lichtenthaler 1986) show peaks only in red, and at wavelengths characteristically longer than corresponding absorption peaks, namely 648 cf. 642 nm for Chl *b*, and 668 cf. 662 nm for Chl *a*. Lower curves: In situ absorption spectra (eluted from gel slices) for pigment-protein complexes corresponding to photosystem II reaction centre (PSII RC) and light-harvesting chlorophyll (*a*,*b*)-protein complexes (LHC). A secondary peak at 472 nm and a shoulder at 653 nm indicate contributions from Chl b to these broadened absorption spectra which have been normalised to 10 µM Chl solutions in a 1 cm path length cuvette. (Based on from Evans and Anderson 1987)

Chlorophylls are readily extracted from (soft) leaves into organic solvent and separated chromatographically into constituent types, most notably

chlorophyll *a* (Chl *a*) and chlorophyll *b* (Chl *b*). These two chemical variants of chlorophyll are universal constituents of wild vascular plants and express highly characteristic absorption spectra (Figure 1.8). Both chlorophylls show absorption maxima at wavelengths corresponding to blue and red, but chlorophyll assay in crude extracts, which inevitably contain carotenoids as well, is routinely based on absorption maxima in red light to avoid overlap with these accessory pigments that show strong absorption below 500 nm. Absorption maxima at 659 and 642 for Chl *a* and Chl *b* respectively would thus serve for assay in diethylether, but these peaks will shift slightly according to solvent system, and such shifts must be taken into account for precise measurement (see Porra *et al.* 1989 for details).

Chl *a* and Chl *b* differ with respect to both role and relative abundance in higher plants. Chl *a*/*b* ratios commonly range from 3.3 to 4.2 in well-nourished sun-adapted species, but can be as low as 2.2 or thereabouts in shade-adapted species grown at low light. Such variation is easily reconciled with contrasting functional roles for both Chl *a* and Chl *b*. Both forms of chlorophyll are involved in light harvesting, whereas special forms of only Chl *a* are linked into energy-processing centres of photosystems. In strong light, photons are abundant, consistent with a substantial capacity for energy processing by leaves (hence the higher Chl *a*/*b* ratio). In weak light, optimisation of leaf function calls for greater investment of leaf resources in light harvesting rather than energy processing. As a result the relative abundance of Chl *b* will increase and the Chl *a*/*b* ratio will be lower compared with that in strong light. As a further subtlety, the two photosystems of higher plant chloroplasts (discussed later) also differ in their Chl *a*/*b* ratio, and this provided Boardman and Anderson (1964) with the first clue that they had achieved a historic first in the physical separation of those two entities.

Carotenoids also participate in photosynthetic energy transduction. Photosystems have an absolute requirement for catalytic amounts of these accessory pigments, but their more substantive involvement is via dissipation of potentially harmful energy that would otherwise impact on delicate reaction centres when leaves experience excess photon irradiance (further details in Chapter 12). Carotenoids are thus regarded as ‘accessory’ to primary pigments (chlorophylls) and in molar terms are present in mature leaves at about one-third the abundance of Chl (*a* + *b*).

Obviously, chlorophyll in leaves is not in solution but exists in a gel-like state where all pigment molecules are linked to proteins, and absorption spectra differ accordingly (see Evans and Anderson 1987). In particular, light-harvesting Chl *a*, *b*–protein complexes (LHC in Figure 1.8, lower curves) develop a secondary absorption peak at 472 nm with a shoulder at 653 nm, while the Chl *a* of photosystem II reaction centres shows absorption peaks at 437 and 672 nm (compared with 429 and 659 nm for purified Chl *a* in ether; Figure 1.8, upper curves).

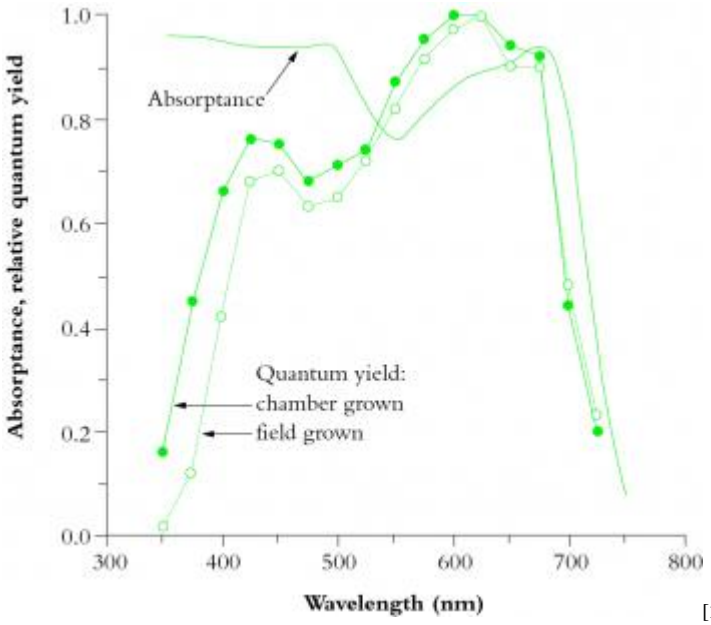

[13]

Figure 1.9 Leaves absorb visible light very effectively (>90% for all wavelengths combined; solid curve).Wavelengths corresponding to green light are absorbed less effectively (absorptance drops to c. 0.75). Beyond 700 nm (infrared band) absorptance drops to near zero, and forestalls leaf heating from this source of energy. Quantum yield is referenced to values obtained in red light (600-625 nm), which is most effective in driving photosynthesis, requiring about 10 quanta per CO_2assimilated (based on high-precision leaf gas exchange) compared with about 12 quanta at the blue peak (450 nm). Quantum yield shows a bimodal response to wavelength. Absorptance drops beyond 700 nm but quantum yield drops off even faster because PSII (responsible for O_2 generation) absorbs around 680 nm and cannot use quanta at longer wavelengths in this measuring system. UV wavelengths (below 400 nm) are capable of driving photosynthesis, but as a protective adaptation vascular plants accumulate a chemical 'sunscreen' in response to UV exposure. Field-grown plants are especially rich in these substances so that absorbed UV is dissipated harmlessly, lowering quantum yield compared with growth-chamber plants. (Based on McCree 1972)

Subtle alterations in the molecular architecture of chlorophyll molecules according to the particular protein to which they bind in either light-harvesting or energy-processing centres are responsible for these shifts in absorption peaks, and for a general broadening of absorption spectra (compare lower and upper curves in Figure 1.8). Such effects are further accentuated within intact leaves by accessory pigments and greatly lengthened absorption pathways resulting in about 85% of visible wavelengths being absorbed (Figure 1.9). Any absorbed quanta at wavelengths below 680 nm can drive one electron through either reaction centre. Maximum quantum yield (Figure 1.9) occurs when both reaction centres absorb equal numbers of such quanta. When one photosystem population (PSII) absorbs more quanta than the other (PSI), excess quanta cannot be used to drive whole-chain (linear) electron flow. Quantum yield is reduced as a consequence, and leads to a slight discrepancy between *in vivo* absorption maxima (Figure 1.8) and quantum yield (Figure 1.9).

Although UV wavelengths are absorbed by leaves and would be capable of driving photosynthesis, such short wavelengths are damaging to biological systems and plants have adapted by developing a chemical sunscreen. Consequently, the quantum yield from these wavelengths drops off markedly below about 425 nm. Beyond 700 nm (infrared band) absorption drops to near zero, and forestalls leaf heating from this source of energy. However, quantum yield falls away even faster, and this 'red drop', though puzzling at first, led subsequently to a comprehensive model for photosynthetic energy transduction, outlined below.

1.2.3 Cooperative photosystems and a 'Z' scheme for electron flow

Prior to the advent of high-precision leaf gas exchange methods (as employed for Figure 1.9), O_2 evolution was taken as a measure of photosynthetic activity. Action spectra were measured on a number of plants and algae over the range of visible radiation. A crucial and consistent observation was that O_2 evolution dropped off much faster in the long-wavelength red region (>690 nm) than did absorption. Put another way, more quanta were being absorbed at longer wavelengths than could be used for photosynthesis. It seemed at these longer wavelengths as though a light absorber was being robbed of energy-processing capacity.

Anticipating that bimodal absorption implied a two-step process, and knowing that chlorophyll also absorbed photons at shorter wavelengths, Robert Emerson (working at Urbana in the mid-1950s) supplemented far-red light with shorter wavelength red irradiance and demonstrated that the relatively low photosynthetic rate in far-red light could be significantly increased. In fact the photosynthetic rate achieved with the two light qualities combined could be 30–40% higher than the sum of the rates in far-red or shorter red when measured separately (Emerson *et al.* 1957). This phenomenon became known as the 'Emerson Enhancement Effect' and contributed to a working hypothesis for photo-synthetic energy conversion based upon two photochemical acts (proposed by Duysens *et al.* 1961), but additional lines of evidence were impacting on this outcome.

At about the same time as Emerson was establishing his enhancement effect, Myers and French observed 'sequential enhancement'; that is, a disproportionate increase in photosynthetic rate or efficiency when the two light qualities were separated in time. The upper limits of dark intervals between two flashes of different light quality were 6 s for far-red after green and and 1 min for green after far-red. Clearly, the 'product' of photochemical act 1 was stable for 1 min, that of act 2 for only 6 s. This discovery implied that chemical intermediates, rather than an altered physical state, were involved in a two-step cooperation (see Clayton 1980).

According to physical laws of photochemical equivalence, there should be a 1:1 yield in converting light energy to chemical energy by a perfect system. Quantum requirement for such events would be 1. However, in photosynthesis the absolute quantum requirement for O_2 evolution was clearly much greater than 1 and though contentious at first proved to be somewhere between 8 and 10. Such requirement implied a multistep process for energy conversion. Indeed, during the early 1940s a scientific controversy raged between Otto Warburg (Berlin) and Robert Emerson (Urbana) about the quantum requirement of photosynthesis in green algae and plants. Using manometry, a technique predating O_2electrodes, Warburg related rates of O_2 evolution to absorbed quanta and claimed that 4 quanta were sufficient for the evolution of one molecule of O_2. By contrast, Emerson and many other scientists were reporting values of 6 to 12 quanta per molecule of O_2. The two sets of protagonists agreed to a collaborative effort, and by the late 1950s Emerson and co-workers resolved that 8–10 quanta were required.

How then could multiples of 2 quanta cooperate in the separation of one strong reducing and one strong oxidising equivalent? Everything started coming together when Hill and Bendall (1960) suggested a 'Z' scheme that was not only consistent with a requirement of 8–10 quanta and the 2 quanta cooperation principle, but also the operation of two sequential photochemical acts (Figure 1.10 is a greatly embellished version of their original model).

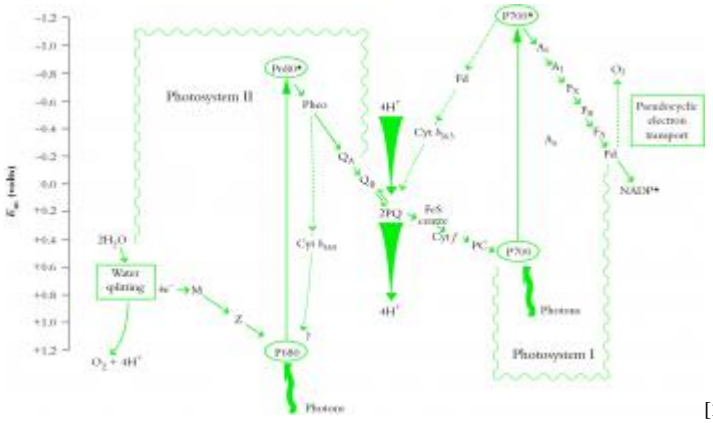

[14]

Figure 1.10 A highly diagrammatic zig-zag or 'Z' scheme of photosynthetic electron transport from water to NADP$^+$showing the sequence of electron/proton carriers and their association with either PSII or PSI. Linear electron flow is shown as solid lines; cyclic electron flow is indicated by dashed lines. All of these electron transport chains operate within thylakoid membranes with electron flow following a sequence dictated by redox potential (shown in volts on the ordinate). Cyclic electron flow in PSII diverts electrons from pheophytin to cytochrome *b*559 (and possibly back to P680$^+$). Cyclic electron transport around PSI moves electrons from ferredoxin through cytochrome *b*565 and plastoquinone (PQ), while pseudocyclic electron transport takes electrons from ferredoxin to O_2.

In linear flow, water molecules are split in PSII, liberating $O_2$and providing a source of electrons. M is the manganese—containing cluster which oxidises water, Z is tyrosine-161 of the D1 protein which in turn represents the primary electron donor to P680$^+$ (a special pair of Chl a molecules

with an absorption peak at 680 nm). Pheo is the primary electron acceptor pheophytin *a*, a chlorophyll molecule lacking magnesium; Q_A is the first stable and permanently bound plastoquinone electron acceptor; Q_B is the second, temporarily bound, plastoquinone electron acceptor which actually leaves PSII in a reduced form (PQH_2). Further along, FeS = Rieske iron—sulphur centre; Cyt *f* = cytochrome *f*; PC = plastocyanin; P700 = reaction centre chlorophyll *a* of PSI; A_0, A_1, F_X, F_B and F_A are electron acceptors of PSI; Fd = ferredoxin; Cyt *b*559 = cytochrome *b*559; Cyt *b*563 = cytochrome *b*563. Also shown as tapered arrows is H^+ accumulation in the lumen associated with water and plastoquinol oxidations. (Original drawing courtesy C. Critchley)

The original version of this 'Z' scheme was further validated by unequivocal evidence from Australia that the two (inferred) photosystems were indeed separate physical entities. Using sophisticated biochemical chloroplast purification and subfractionation methods, coupled with detergent solubilisation of membranes, Boardman and Anderson (1964) achieved the first physical separation of photosystem II (PSII) and photosystem I (PSI), thus confirming the separate identities of those complexes.

A source of electrons had long been recognised as basic to the operation of this 'Z' scheme, with H_2O molecules an obvious source, but were photosynthetic membranes capable of photolysis? Early experiments by Robin Hill and colleagues at Cambridge had established this capability. They used isolated thylakoid membrane preparations and showed that O_2 could be evolved in the absence of CO_2 as long as external electron acceptors were present (Hill reaction). Intact leaves or whole chloroplasts have no need for an artificial acceptor because electron flow is directed to $NADP^+$ and subsequent reduction of CO_2 (first demonstrated with intact chloroplasts; see Arnon 1984). The O_2-evolving function of photosynthesis was found to be associated with PSII in experiments with isolated thylakoids using external (artificial) electron donors and acceptors and specific electron transport inhibitors. As one outcome of those early Cambridge experiments, O_2 evolution is now measured routinely *in vitro* (and *in vivo* on leaves) with O_2 electrodes (Walker 1987).

Chloroplast structure and function is by now sufficiently well defined to consider photosynthetic electron flow in detail. Figure 1.10 applies equally well to vascular plants or to algae with oxygenic photosynthesis, where in either case two photosystems work cooperatively and sequentially in absorbing photons and converting their quantum energy into a flow of electrons. Paradoxically, convention has it that photosynthetic electron flow initiates in PSII and proceeds to PSI. PSII was so named because PSI had already been described in single-celled (prokaryotic) organisms and, owing to the rules of nomenclature, was accorded priority.

Both photosystems are large multi-subunit complexes, quite different structurally and functionally, and operating in series. In PSII, electrons are provided from a water-splitting apparatus via a manganese complex which undergoes oxidation

from a valency state of +2 to +4. These oxidation states are made possible by $P680^+$ (a special form of Chl *a* with an absorption peak at 680 nm). $P680^+$ is a powerful oxidant generated by absorption of energy from a photon. P680 is referred to as a 'special pair' because it is a pair of Chl *a* molecules. Electrons from P680 pass to pheophytin (Pheo in Figure 1.10) and on to a bound quinone molecule, Q_A. From there a second transiently bound quinone, Q_B, receives two electrons in succession and requires protonation. The entire, fully reduced, quinone molecule leaves PSII and enters a plastoquinone pool (2PQ).

All of the electron transport cofactors of PSII and one β-carotene are bound to proteins D1 and D2. They in turn form a heterodimer, and together with cytochrome b_{559}, a 9 kDa phosphoprotein and a 22 kDa protein, form the PSII reaction centre. Attached to the reaction centre are core proteins which carry 50 Chl *a* and carotenoid pigments. A heterogeneous light-harvesting chlorophyll–protein complex constitutes an outer antenna system and is composed of trimeric 28 kDa proteins which *in toto* bind 250–300 Chl (*a* + *b*) molecules per reaction centre. These 28 kDa proteins also bind carotenoids which provide one avenue for energy dissipation when photon capture exceeds subsequent energy utilisation (e.g. stressed plants in strong sunlight). Photons absorbed by the many pigments in LHCII are transferred as excitons by the LHCII and core pigments to reaction centres where they are finally trapped by P680. Such 'traps' are regarded as open if Q_A is oxidised and ready to receive an electron from P680. If, however, Q_A is still in its reduced state, that 'trap' will be closed, and excitons will then transfer to another reaction centre or be lost as heat or fluorescence. Traps have about one-billionth of a second (10^{-9} s) to accept an exciton before such energy is lost by either pathway.

In PSI, absorption of quantum energy from a photon causes oxidation of P700, the PSI reaction centre equivalent of P680. In contrast to PSII, where electrons are drawn from a water-splitting apparatus, P700 accepts electrons from PC (reduced form PC^- in Figure 1.11). Electrons then pass through three iron–sulphur (FeS) centres and out of PSI to ferredoxin (Fd). The reaction centre of PSI contains several proteins, but most of the electron transfer cofactors are bound to large heterodimeric proteins which in turn bind the inner Chl *a* antenna. The LHCI complex consists of possibly eight polypeptides of between 24 and 27 kDa which carry Chl *a* and Chl *b* plus carotenoids.

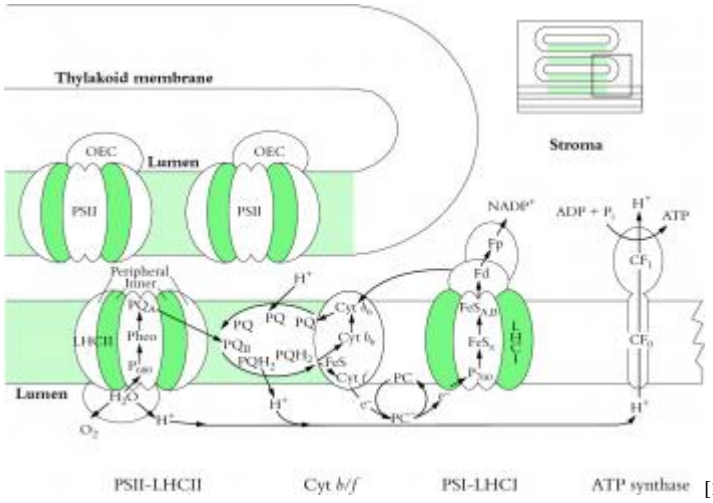

[15]

Figure 1.11 Light harvesting, photosynthetic electron transport from H_2O to $NADP^+$ and generation of ATP are achieved via four types of complexes which show a lateral heterogeneity within thylakoid membranes. A small part of a continuous network of interconnected thylakoids is shown here diagrammatically where PSI complexes and ATP synthase are restricted to non—appressed regions. Most PSII complexes and the light-harvesting assemblages associated with PSII (LHCII) are held within appressed regions of this network. Cytochrome *b/f* complexes (Cyt *b/f*) are more generally located.

A chemiosmotic coupling mechanism is responsible for ATP synthesis. Protons are 'pumped' across the thylakoid membrane from outside (stroma) to inside (lumen) by a complex arrangement of electron carriers embedded within the membrane. A prodigious concentration of protons builds up within the lumen, partly from photolysis of water molecules (water-splitting apparatus on PSII) and partly from oxidation of plastoquinone (PQ) on the inner face of the membrane.This protonmotive force from inside (lumen) to outside (stroma) is used to generate ATP within the stroma via an ATP synthase complex that straddles the thylakoid membrane. OEC = oxygen-evolving complex; Pheo = pheophytin *a*. (Based on Anderson and Andersson 1988)

These two photosystems are juxtaposed across thylakoid membranes in such a way that linear electron transport is harnessed for charge separation, leading to a massive accumulation of H^+ ions within the lumen of illuminated thylakoids, which is then employed in ATP generation.

Combining concepts of photolysis and photosynthetic electron flow outlined earlier (Figure 1.10) and putting that conceptual framework into a thylakoid membrane system (Figure 1.11), a picture emerges where electrons generated from splitting H_2O molecules on the inner surface of PSII are transferred from plastoquinol (PQH_2) to the Rieske iron– sulphur centre (Rieske FeS) of the cytochrome b_6/f complex (Cyt b_6/f) and further to cytochrome *f* (Cyt *f*). The pivotal importance of Cyt *f* in facilitating electron transport from PSII to PSI was demonstrated by Duysens and colleagues (see Levine 1969), who showed that preferential energisation of PSII (light at <670 nm) caused reduction, whereas preferential energisation of PSI (light at >695 nm) caused oxidation. This elegant

'push–pull' experiment confirmed the cooperative and sequential nature of PSII and PSI, as well as indicating overall direction of photosynthetic electron flow.

Proteins which bind the Rieske FeS centre and Cyt *f* together with cytochrome b_{563} (Cyt b_6) form a large electron transfer complex. This complex (Figure 1.11) spans the membrane and is located between the two photosystems. Electrons are transferred to PC (forming PC^-), a copper-containing soluble protein extrinsic to the thylakoid membrane and located in the lumen. On the other side of the membrane, attached to the stromal side, is ferredoxin (Fd) which accepts electrons from PSI and passes them on to ferredoxin–NADP reductase, an enzyme, also extrinsic to thylakoids, and attached on the stromal side of the thylakoid membrane. This enzyme accomplishes the final electron transfer in an overall linear chain and reduced NADP is then protonated.

While linear electron transport from water to $NADP^+$ is the main and most important path, electrons can also be transferred to O_2 in a so-called pseudocyclic or Mehler reaction (Figure 1.10). This pathway probably operates *in vivo* as a sink for electrons when synthetic events call for more ATP than NADPH. Electrons can also be cycled around both PSII and PSI. Electrons cycling around PSI will produce ATP but with no accompanying NADPH. Cyclic electron flow around PSII may have a completely different role and may be related to the downregulation of this photosystem during photoinhibition (Chapter 12).

According to this multistage scheme, electrons are transferred from donor (reductant) to acceptor (oxidant). The direction of that transfer depends upon a difference in oxidation–reduction potential between a given donor and a given acceptor (as indicated on the ordinate in Figure 1.10). A more positive potential implies stronger oxidative power (i.e. capacity to accept electrons); a more negative potential implies stronger reducing power (i.e. capacity to donate electrons). P680* thus has a strong capacity to donate electrons (a strong reductant); P700* has an even stronger capacity to donate electrons (an even stronger reductant).

Molecules which accept electrons are immediately protonated. In aqueous systems, such as chloroplasts *in vivo*, hydrogen ions (H^+) are ubiquitous, and these ions combine with electron acceptors to generate hydrogen atoms (i.e. H^+ ion + electron → H atom). In Figure 1.10, some events involve electron transfer, while others include transfer of hydrogen atoms. As a simplifying convention, all such events are referred to as electron transfers. Ironically, the end result of all these reactions is a net transfer of hydrogen atoms!

1.2.4 Photophosphorylation and ATP synthesis

During photosynthetic electron transfer from water to $NADP^+$, energy captured in two photoacts is stored as an electrochemical potential gradient of protons. First, such reduction of Q_B requires protonation with protons drawn from the stromal side of the membrane. Reoxidation (and deprotonation) occurs towards the thylakoid lumen. In addition, protons are lost from the stromal side via protonation of reduced NADP and they are also generated in the lumen during photolysis. A massive ΔpH, of approximately 3–4 pH units, equivalent to an H^+ ion concentration difference of three to four orders of magnitude, develops across the thylakoid membrane. This immense gradient drives ATP synthesis (catalysed by ATP synthase) within a large energy-transducing complex embedded in the thylakoid membrane (Figure 1.11).

ATP synthesis in chloroplasts (photophosphorylation) proceeds according to a mechanism that is basically similar to that in mitochondria. Chemiosmotic coupling (Mitchell 1961) which links the movement of protons down an electro-chemical potential gradient to ATP synthesis via an ATP synthase applies in both organelles. However, the orientation of ATP synthase is opposite. In chloroplasts protons accumulate in thylakoid lumen and pass outwards through the ATP synthase into the stroma. In mitochondria, protons accumulate within the intermembrane space and move inwards, generating ATP and oxidising NADH within the matrix of these organelles (Figure 2.24).

In chloroplasts, ATP synthase is called the CF_0CF_1 complex. The CF_0 unit is a hydrophobic transmembrane multiprotein complex which contains a water-filled proton conducting channel. The CF_1 unit is a hydrophilic peripheral membrane protein complex that protrudes into the stroma. It contains a reversible ATPase and a gate which controls proton movement between CF_0 and CF_1. Entire CF_0CF_1complexes are restricted to non-appressed portions of thylakoid membranes due to their bulky CF_1 unit.

Direct evidence for ATP synthesis due to a transthylakoid pH gradient can be adduced as follows. When chloroplasts are stored in darkness in a pH 4.0 succinic acid buffer (i.e. a proton-rich medium), thylakoid lumen equilibrate to this pH. If the chloroplasts, still in the dark, are rapidly transferred to a pH 8.0 buffer containing ADP and P_i, ATP synthesis then occurs. This outcome confirms a central role for the proton concentration difference between thylakoid lumen and stroma for ATP synthesis *in vitro*; but does such a process operate on that scale *in vivo*?

Mordhay Avron, based in Israel, answered this question in part during the early 1970s via a most elegant approach (Rottenberg *et al*. 1972). Working with thylakoid preparations, Avron and colleagues established that neutral amines were free to exchange between bathing medium and thylakoid lumen, but once protonated in illuminated preparations they became trapped inside. By titrating the loss of such amines from the external medium when preparations where shifted

from dark to light, they were able to infer the amount retained inside. Knowing that the accumulation of amine depended upon H^+ ion concentration in that lumen space, the difference in H^+ ion concentration and hence ΔpH across the membrane were established.

At saturating light, chloroplasts generate a proton gradient of approximately 3.5 pH units across their thylakoid membranes. Protons for this gradient are derived from the oxidation of water molecules occurring towards the inner surface of PSII and from transport of four electrons through the Cyt *b*/*f* complex, combined with cotranslocation of eight protons from the stroma into the thylakoid space for each pair of water molecules oxidised. Electrical neutrality is main-tained by the passage of Mg^{2+} and Cl^- across the membrane, and as a consequence there is only a very small electrical gradient across the thylakoid membrane. The electrochemical potential gradient that yields energy is thus due almost entirely to the concentration of intrathylakoid H^+ ions.

For every three protons translocated via ATP synthase, one ATP is synthesised. Linear electron transport therefore generates about four molecules of ATP per O_2 evolved. Thus eight photons are absorbed for every four ATP molecules generated or for each O_2 generated. Cyclic electron transport is slightly more efficient at producing ATP and generates about four ATP per six photons absorbed. However, linear electron transport also generates NADPH, which is equivalent, in energy terms, to six ATP per O_2 released.

As implied in Figure 1.11, the four thylakoid complexes, PSII, PSI, Cyt *b*/*f* and ATP synthase, are not evenly distributed in plant thylakoid membranes but show a lateral heterogeneity. This distribution is responsible for the highly characteristic structural organisation of the continuous thylakoid membrane into two regions, one consisting of closely appressed membranes or granal stacks, the other of non-appressed stroma lamellae where outside surfaces of thylakoid membranes are in direct contact with the stroma. This structural organisation is shown on a modest scale in Figure 1.7, but extreme examples are evident in chloroplasts of shade-adapted species grown in low light (Chapter 12). Under such conditions, membrane regions with clusters of PSII complexes and Cyt *b*/*f* complexes become appressed into classical granal stacks. Cyt *b*/*f* complexes are present inside these granal stacks as well as in stroma lamellae, but PSI and ATP synthase are absent from granal stacks. Linear electron transport occurs in granal stacks from PSII in appressed domains to PSI in granal margins. Nevertheless, shade plants have only a low rate of linear electron transport because they have fewer Cyt *b*/*f* and to a lesser extent fewer PSII complexes compared to PSI, a consequence of investing more chlorophyll in each PSII to enhance light harvesting (see Anderson (1986) and Chapter 12 for more detail).

1.2.5 Chlorophyll fluorescence

A dilute solution of leaf chlorophyll in organic solvent appears green when viewed with light transmitted from a white source. Wavelengths corresponding to bands of blue and red have been strongly absorbed (Figure 1.8), whereas mid-range wavelengths corresponding to green light are only weakly absorbed, hence the predominance of those wavelengths in transmitted and reflected light. However, viewed laterally via re-emitted energy, the solution will appear deep red, and that same colour will persist regardless of source light quality. Fluorescence spectra are invariate, and the same spectrum will be obtained (e.g. Figure 1.8 inset) regardless of which wavelengths are used for excitation. This characteristic emission is especially valuable in establishing source pigments responsible for given emission spectra, and for studying changes in their photochemical status during energy transduction.

Fluorescence emission spectra (Figure 1.8 inset) are always displaced towards longer wavelengths compared with corresponding absorption spectra (Stoke's shift). As quantum physics explains, photons intercepted by the chromophore of a chlorophyll molecule cause an instantaneous rearrangement of certain electrons, lifting that pigment molecule from a ground state to an excited state which has a lifetime of *c*. 10^{-9} s. Some of this excitation energy is subsequently converted to vibrational energy which is acquired much more 'slowly' by much heavier nuclei. A non-equilibrium state is induced, and molecules so affected begin to vibrate rather like a spring with characteristic periodicity, leading in turn to energy dissipation as heat plus remission of less energetic photons of longer wavelength.

Apart from their role in photon capture and transfer of excitation energy, photosystems function as energy converters because they are able to seize photon energy rather than lose as much as 30% of it through fluorescence as do chlorophylls in solution. Moreover, they can use the trapped energy to lift an electron to a higher energy level from where it can commence a 'downhill' flow via a series of electron carriers as summarised in Figure 1.10.

Protein structure confers very strict order on bound chlorophylls. X-ray crystallographic resolution of the bacterial reaction centre has given us a picture of the beautiful asymmetry of pigment and cofactor arrangements in these reaction centres, and electron diffraction has shown us how chlorophylls are arranged with proteins that form the main light-harvesting complexes of PSII. This structural constraint confers precise distance and orientation relationships between the various chlorophylls, as well as between chlorophylls and carotenoids, and between chlorophylls and cofactors enabling the photosystems to become such effective photochemical devices. It also means that only 2–5% of all the energy that is absorbed by a photosystem is lost as fluorescence.

If leaf tissue is held at liquid nitrogen temperature (77 K), photosynthetic electron flow ceases and chlorophyll fluorescence does increase, including some emission from PSI. Induction kinetics of chlorophyll fluorescence at 77 K have been used to

probe primary events in energy transduction, and especially the functional state of photosystems. Present discussion is restricted to room temperature fluorescence where even the small amount of fluorescence from PSII is diagnostic of changes in functional state. This is because chlorophyll fluorescence is not emitted simply as a burst of red light following excitation, but in an ordered fashion that varies widely in flux during continuous illumination. These transient events (Figure 1.12) are referred to collectively as fluorescence induction kinetics, fluorescence transients, or simply a Kautsky curve in honour of its discoverer Hans Kautsky (Kautsky and Franck 1943).

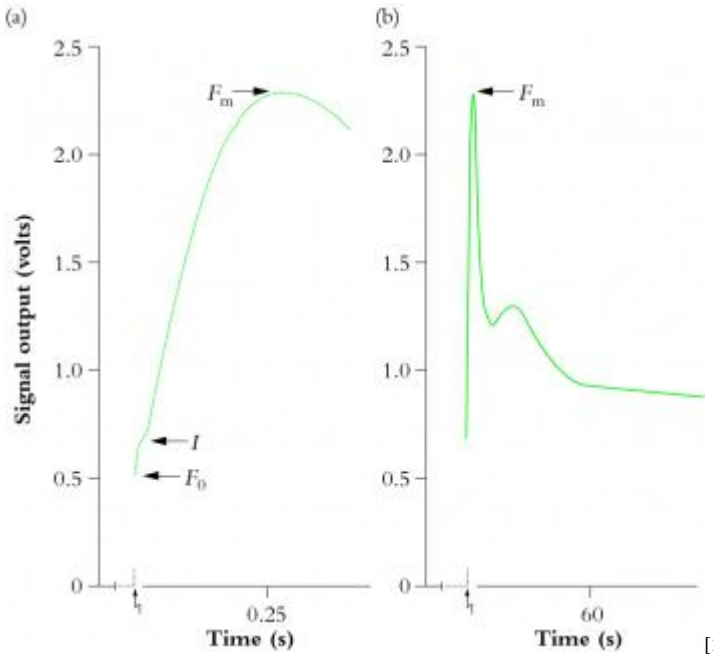

[16]

Figure 1.12 A representative chart recorder trace of induction kinetics for Chl a fluorescence at room temperature from a mature bean leaf (*Phaseolus vulgaris*). The leaf was held in darkness for 17 min prior to excitation (zig-zag arrow) at a photon irradiance of 85 µmol quanta m^{-2} s^{-1}. The overall Kautsky curve is given in (b), and an expanded version of the first 400 ms is shown in (a). See text for explanation of symbols and interpretation of variation in strength for these 'rich but ambiguous signals'! (Based on Norrish et al. 1983; reproduced with permission of Kluwer Academic Publishers)

At room temperature and under steady-state conditions, *in vivo* Chl *a* fluorescence from an immature (greening) bean leaf shows a characteristic emission spectrum with a distinct peak around 680–690 nm and a shoulder near 735 nm. As leaf chlorophyll concentration increases, the intensity of fluorescence at 680–690 nm diminishes compared with emission at 735 nm due to reabsorption of shorter wavelengths by the extra chlorophyll molecules. Fully developed bean leaves thus show a new maximum between 730 and 740 nm. Room temperature fluorometers rely on this secondary peak.

(a) Fluorescence induction kinetics

Strength of emission under steady-state conditions varies according to the fate of photon energy captured by LHCII, and the degree to which energy derived from photosynthetic electron flow is gainfully employed. However, strength of emission fluctuates widely during induction (Figure 1.12) and these rather perplexing dynamics are an outcome of some initial seesawing between photon capture and subsequent electron flow. Taking Figure 1.10 for reference, complexities of a fluorescence transient (Figure 1.12) can be explained as follows. At the instant of excitation (zig-zag arrow), signal strength jumps to a point called F_0 which represents energy derived largely from chlorophyll molecules in the distal antennae of the LHCII complex which fail to transfer their excitation energy to another chlorophyll molecule, but lose it immediately as fluorescence. F_0 thus varies according to the effectiveness of coupling between antennae chlorophyll and reaction centre chlorophyll, and will increase due to high-temperature stress or photodamage. Manganese-deficient leaves show a dramatic increase in F_0 due to loss of functional continuity between photon-harvesting and energy-processing centres of PSII (discussed further in Chapter 16).

Returning to Figure 1.12, the slower rise subsequent to F_0 is called *I*, and is followed by a further rise to F_m. These stages reflect a surge of electrons which fill successive pools of various electron acceptors of PSII. Significantly, F_m is best expressed in leaves that have been held in darkness for at least 10–15 min. During this dark pretreatment, electrons are drawn from Q_A, leaving this pool in an oxidised state and ready to accept electrons from PSII. An alternative strategy is to irradiate leaves with far-red light to energise PSI preferentially, and so draw electrons from PSII via the Rieske FeS centre. The sharp peak (F_m) is due to a temporary restriction on electron flow downstream from PSII. This constraint results in maximum fluorescence out of PSII at about 500 ms after excitation in Figure 1.12(a). That peak will occur earlier where leaves contain more PSII relative to electron carriers, or in DCMU-treated leaves.

Photochemistry and electron transport activity always quench fluorescence to a major extent unless electron flow out of PSII is blocked. Such blockage can be achieved with the herbicide 3-(3,4-dichlorophenyl)-1,1-dimethyl urea (DCMU) which binds specifically to the D1 protein of PSII and blocks electron flow to Q_B. DCMU is a very effective herbicide because it inhibits photosynthesis completely. As a consequence, signal rise to F_m is virtually instantaneous, and fluorescence emission stays high.

Variation in strength of a fluorescence signal from F_0 to F_m is also called variable fluorescence (F_v) because scale and kinetics of this rise are significantly influenced by all manner of environmental conditions. F_0 plus F_v constitute the maximal fluorescence (F_m) a leaf can express within a given measuring system.
The F_v/F_m ratio, measured after dark treatment, therefore reflects the proportion of efficiently working PSII units among the total PSII population. Hence it is a

measure of the photochemical efficiency of a leaf, and correlates well with other measures of photosynthetic effectiveness (discussed further in Chapter 12).

(b) Fluorescence relaxation kinetics

Excellent fluorometers for use in laboratory and field such as the Plant Efficiency Analyser (Hansatech, King's Lynn, UK) make accurate measurements of all the indices of the Kautsky curve and yield rapid information about photochemical capacity and response to environmental stress.

Even more sophisticated is the Pulse Amplitude Modulated (PAM) fluorometer (Walz, Effeltrich, Germany) which employs a number of fluorescence- and/or photosynthesis-activating light beams and probes fluorescence status and quenching properties. With induction kinetics generated by conventional fluorometers (e.g. Figure 1.12) a given source of weak light (commonly a red light-emitting diode producing only 50–100 µmol quanta m^{-2} s^{-1}) is used for both chlorophyll excitation and as a source of light for photosynthetic reactions. By contrast a PAM fluorometer measures fluorescence excited by a weak modulated light and applies pulses of saturating light for chlorophyll excitation on top of an actinic beam which sustains photosynthesis. A combination of optical filters plus sophisticated electronics ensures that detection of fluorescence emission is locked exclusively onto the modulated signal. In this way, most of the continuous background fluorescence and reflected long-wavelength light is disregarded. The functional condition of PSII in actively photosynthesising leaf tissue is thus amenable to analysis. This instrument also reveals the relative contributions to total fluorescence quenching by photochemical and non-photochemical processes and will help assess any sustained loss of quantum efficiency in PSII. Photosynthetic electron transport rates can be calculated concurrently.

Photochemical quenching (q_p) varies according to the oxidation state of electron acceptors on the donor side of PSII. When Q_A is oxidised (e.g. subsequent to dark pretreatment), quenching is maximised. Equally, q_p can be totally eliminated by a saturating pulse of excitation light that reduces Q_A, so that fluorescence yield will be maximised, as in a PAM fluorometer. Concurrently, a strong beam of actinic light drives photosynthesis (maintaining linear electron flow) and sustaining a pH gradient across thylakoid membranes for ATP synthesis. Those events are a prelude to energy utilisation and contribute to non-photochemical quenching (q_n). This q_n component can be inferred from a combination of induction plus relaxation kinetics.

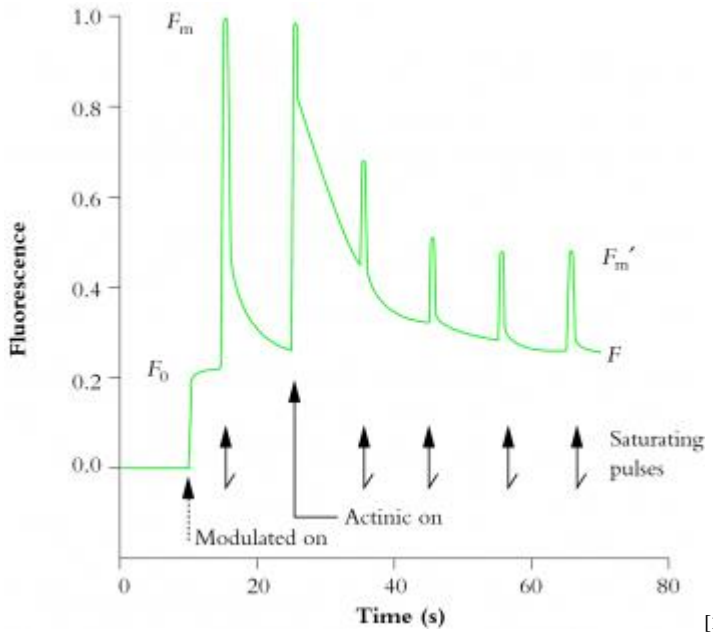

[17]

Figure 1.13 Induction and relaxation kinetics of *in vivo* Chl a fluorescence from a well-nourished radish leaf (*Raphanus sativus*) supplied with a photon irradiance of actinic light at 500 µmol quanta m^{-2} s^{-1} and subjected to a saturating pulse of 9000 µmol quanta m^{-2} s^{-1} for 0.8 s every 10 s. Output signal was normalised to 1.0 around the value for F_m following 30 min dark pretreatment. Modulated light photon irradiance was <1 µmol quanta m^{-2} s^{-1}. See text for definition of symbols and interpretation of kinetics . (Original (unpublished) data from John Evans generated on a PAM fluorometer (Heinz Walz GmbH, Germany))

In Figure 1.13, a previously darkened radish leaf (traps now open and Q_A oxidised) initially receives weak modulated light (<1 µmol quanta m^{-2} s^{-1}) that is insufficient to close traps but sufficient to establish a base line for constant yield fluorescence (F_0). This value will be used in subsequent calculations of fluorescence indices. The leaf is then pulsed with a brief (0.8 s) saturating flash (9000 µmol quanta m^{-2} s^{-1}) to measure F_m. Pulses follow at 10 s intervals to measure F_m9. Actinic light (500 µmol quanta m^{-2} s^{-1}) starts with the second pulse and DpH starts to build up in response to photosynthetic electron flow. Photosynthetic energy transduction comes to equilibrium with these conditions after a minute or so, and fluorescence indices q_n and q_p can then be calculated as follows:

$$q_n = (F_m - F_m')/(F_m - F_0), \text{ and}$$
$$q_p = (F_m' - F_0)/(F_m' - F_0) \qquad (1.1)$$

Under these steady-state conditions, saturating pulses of excitation energy are being used to probe the functional state of PSII, and by eliminating q_p the quantum efficiency of light-energy conversion by PSII (Φ_{PSII}) can be inferred:

$$\Phi_{PSII} = (F_m' - F)/(F_m') \qquad (1.2)$$

If overall quantum efficiency for O_2 evolution is taken as 10 (discussed earlier), then the rate of O_2 evolution by this radish leaf will be:

$$\Phi_{PSII} \times \text{photon irradiance}/10\ (\mu\text{mol O}_2\ \text{m}^{-2}\text{s}^{-1}) \qquad (1.3)$$

In summary, chlorophyll fluorescence at ambient temperature comes mainly from PSII. This photosystem helps to control overall quantum efficiency of electron flow and its functionality changes according to environmental and internal controls. In response to establishment of a ΔpH across thylakoid membranes, and particularly when irradiance exceeds saturation levels, some PSII units become down-regulated, that is, they change from very efficient photochemical energy converters into very effective energy wasters or dissipators (Chapter 12). Large amounts of the carotenoid pigment zeaxanthin in LHCII ensure harmless dissipation of this energy as heat (other mechanisms may also contribute). PSII also responds to feedback from carbon metabolism and other energy-consuming reactions in chloroplasts, and while variation in pool size of phosphorylated intermediates has been implicated, these mechanisms are not yet understood.

1.3 Concluding remarks

Chloroplasts are sites of solar energy absorption and subsequent transduction into chemically usable forms. Splitting water molecules and developing a protonmotive force of sufficient magnitude to drive ATP synthesis are energy-intensive processes. Consequently, photosynthetic organisms evolved with dual photosystems that work cooperatively and sequentially to extract sufficient quantum energy from parcels of absorbed photons to generate a sufficiently strong electrochemical potential gradient to synthesise the relatively stable, high-energy compounds ATP and NADPH. Such metabolic energy sustains cycles of photosynthetic carbon reduction (PCR) where CO_2 is initially assimilated by one of three photo-synthetic pathways, namely C_3, C_4 or CAM, but eventually fixed via a PCR cycle within the stromal compartment of chloroplasts (considered further in Section 2.1).

Thermodynamically, the net outcome of photosynthetic energy transduction must be viewed as long-term storage of energy in the form of a *product pair*, namely free oxygen and reduced carbon (organic matter), rather than as separate molecules. Plants themselves or indeed any heterotrophic organisms subsequently retrieve such energy via metabolic ‘combustion’ of the organic matter where enzyme-catalysed reactions bring this pair of products together again. These sets of events are outlined in Section 2.4.

Further reading

Evans, J.R. and Caemmerer, S. von (1996). 'Carbon dioxide diffusion inside leaves', *Plant Physiology* **110**, 339-346.

Sharkey TD. (1985). 'Photosynthesis in intact leaves of C_3 plants: physics, physiology and rate limitations' *The Botanical Review*, **51**, 53-105.

Syvertsen, J.P, Lloyd, J., McConchie, C., Kriedemann, PE. and Farquhar, G.D. (1995). 'On the relationship between leaf anatomy and CO_2 diffusion through the mesophyll of hypostomatous leaves', *Plant, Cell and Environment*, **18**, 149-157.

Terashima, I. (1989). 'Productive structure of a leaf', in *Photosynthesis*, ed. WR. Briggs, 207-226, Alan R Liss: New York.

Links:
[1] http://plantsinaction.science.uq.edu.au/edition1//?q=figure_view/16
[2] http://plantsinaction.science.uq.edu.au/edition1//?q=figure_view/968
[3] http://plantsinaction.science.uq.edu.au/edition1//?q=figure_view/17
[4] http://plantsinaction.science.uq.edu.au/edition1//?q=figure_view/18
[5] http://plantsinaction.science.uq.edu.au/edition1//?q=figure_view/19
[6] http://plantsinaction.science.uq.edu.au/edition1//?q=figure_view/20
[7] http://plantsinaction.science.uq.edu.au/edition1//?q=figure_view/22
[8] http://plantsinaction.science.uq.edu.au/edition1//?q=figure_view/46
[9] http://plantsinaction.science.uq.edu.au/edition1//?q=figure_view/37
[10] http://plantsinaction.science.uq.edu.au/edition1//?q=figure_view/38
[11] http://plantsinaction.science.uq.edu.au/edition1//?q=figure_view/48
[12] http://plantsinaction.science.uq.edu.au/edition1//?q=figure_view/52
[13] http://plantsinaction.science.uq.edu.au/edition1//?q=figure_view/53
[14] http://plantsinaction.science.uq.edu.au/edition1//?q=figure_view/54
[15] http://plantsinaction.science.uq.edu.au/edition1//?q=figure_view/55
[16] http://plantsinaction.science.uq.edu.au/edition1//?q=figure_view/56
[17] http://plantsinaction.science.uq.edu.au/edition1//?q=figure_view/58